# Timing of Contractional Stress Propagation, From the Pyrenean Orogen to the Intraplate Domain, Evidenced by U-Pb Dating of Syn-Kinematic Calcite

Agathe Jullien-sicre, Yves Missenard, Thomas Blaise, Romain Augier, Oriane Parizot, Frédéric Haurine

▶ **To cite this version:**

Agathe Jullien-sicre, Yves Missenard, Thomas Blaise, Romain Augier, Oriane Parizot, et al.. Timing of Contractional Stress Propagation, From the Pyrenean Orogen to the Intraplate Domain, Evidenced by U-Pb Dating of Syn-Kinematic Calcite. Tectonics, 2025, 44 (2), ⟨10.1029/2024TC008634⟩. ⟨insu-04974387⟩

**HAL Id: insu-04974387**

**https://insu.hal.science/insu-04974387v1**

Submitted on 3 Mar 2025

**HAL** is a multi-disciplinary open access archive for the deposit and dissemination of scientific research documents, whether they are published or not. The documents may come from teaching and research institutions in France or abroad, or from public or private research centers.

L'archive ouverte pluridisciplinaire **HAL**, est destinée au dépôt et à la diffusion de documents scientifiques de niveau recherche, publiés ou non, émanant des établissements d'enseignement et de recherche français ou étrangers, des laboratoires publics ou privés.

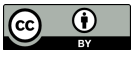

Distributed under a Creative Commons CC BY 4.0 - Attribution - International License

Check for updates

Tectonics®

RESEARCH ARTICLE
10.1029/2024TC008634

**Special Collection:**
Fold-and-Thrust Belts: Evolution and Dynamics at All Spatiotemporal Scales

# Timing of Contractional Stress Propagation, From the Pyrenean Orogen to the Intraplate Domain, Evidenced by U-Pb Dating of Syn-Kinematic Calcite

**Agathe Jullien-Sicre[1], Yves Missenard[1], Thomas Blaise[1], Romain Augier[2], Oriane Parizot[3], and Frédéric Haurine[1]**

[1]CNRS, GEOPS, Université Paris-Saclay, Orsay, France, [2]Institut des Sciences de la Terre d'Orléans (ISTO), UMR, Université d'Orléans, Orléans, France, [3]Université Côte d'Azur, CNRS, OCA, IRD, UMR Géoazur, Sophia Antipolis, France

**Key Points:**

- U-Pb dating of deformation in the retro-foreland of the Pyrenean belt highlights main tectonic event between ca. 48 and 30 Ma
- Renewal of N-S shortening is also recorded during another distinct period between 17 and 11 Ma after a period of shortening tectonics quiescence
- Far field deformation is recorded in the West European intraplate domain remarkably synchronously with the main Pyrenean event

**Supporting Information:**

Supporting Information may be found in the online version of this article.

**Correspondence to:**

A. Jullien-Sicre,
agathe.jullien-sicre@universite-paris-saclay.fr

**Citation:**

Jullien-Sicre, A., Missenard, Y., Blaise, T., Augier, R., Parizot, O., & Haurine, F. (2025). Timing of contractional stress propagation, from the Pyrenean orogen to the intraplate domain, evidenced by U-Pb dating of syn-kinematic calcite. *Tectonics*, *44*, e2024TC008634. https://doi.org/10.1029/2024TC008634

Received 2 OCT 2024
Accepted 26 JAN 2025

**Author Contributions:**

**Conceptualization:** Agathe Jullien-Sicre
**Formal analysis:** Agathe Jullien-Sicre, Yves Missenard, Romain Augier
**Funding acquisition:** Yves Missenard
**Investigation:** Agathe Jullien-Sicre, Oriane Parizot
**Methodology:** Agathe Jullien-Sicre, Yves Missenard, Thomas Blaise, Romain Augier, Frédéric Haurine

© 2025. The Author(s).
This is an open access article under the terms of the Creative Commons Attribution License, which permits use, distribution and reproduction in any medium, provided the original work is properly cited.

**Abstract** The Mediterranean region provides a natural laboratory for studying complex deformation resulting from body forces and interactions between the convergence of the Africa and Eurasia plates since the Cretaceous. These interactions led to the formation of a mosaic of basins and orogenic domains, whose intrinsically complex evolution over time is still subject to debate. Investigating the timing of deformation recorded on both sides of an orogen, and within the intraplate domain, links local-scale processes to regional geodynamic events. This study combines microstructural analysis and U-Pb dating of syn-kinematic calcite with implications for the timing of contractional stress propagation in the Pyrenean orogen and the whole of western Europe. While many U-Pb dating studies on syn-kinematic calcite have been conducted in the western intraplate domain, the northern part of the Pyrenees remains to be investigated, and, therefore, a strategic study area. This study highlights (a) continuous deformation from ca. 48 Ma to 30 Ma, marking the phase of continental collision between Iberia and Eurasia and (b) a newly evidenced post-orogenic Miocene deformation episode, spanning from ca. 16 to 11 Ma. (c) Through a comparison of U-Pb geochronological data from syn-kinematic calcite in the pro-foreland basin and the intraplate domain, this study shows that deformation occurred simultaneously at the plate boundaries and within a large part of the intraplate domain of the overriding plate. These results provide insights into the geodynamic evolution of the Pyrenean orogen and its implications for Mediterranean geodynamics.

## 1. Introduction

During major tectonic events, it is not only the plate boundaries that record deformation, but also the plate interiors, especially when stresses propagates in relation to continental collision (Dèzes et al., 2004; Dielforder et al., 2019; Willingshofer & Sokoutis, 2009; Willingshofer et al., 2013; Ziegler, 1998; Ziegler et al., 1995). Pinpointing the precise timing of deformation, whether it is synchronous between the pro- and retro-foreland and the intraplate domain, is key to understanding the origin of deformation and plate tectonic movements through time.

While modeling studies on fold-and-thrust belts and foreland basins often concentrate on one side of the orogen (Ershov et al., 2003; Fillon et al., 2013), mechanical models highlight a strong mechanical coupling between the pro- and retro-foreland basin in doubly vergent orogens, which is evidenced by the migration of depocentres (Erdős et al., 2015; Hoth et al., 2008; Willett et al., 1993). Slow and prolonged subsidence recorded in retro-foreland basins generally suggests that shortening is mainly accommodated in pro-foreland basins (Sinclair, 2005). However, studies based on cross-section balancing and structural analysis in the eastern Pyrenean pro-wedge and –foreland (Lopez-Blanco et al., 2000; Puigdefàbregas & Souquet, 1986; Vergés et al., 1995), and more recently, in the retro-wedge and foreland (Grool et al., 2018), show that strain distribution on either side is not necessarily synchronous throughout the orogen history. Recent calcite U-Pb geochronology successfully dated deformation in the Southern Pyrenees focusing respectively on fold growth in the Boixols-Sant Corneli anticline (Muñoz-López et al., 2022), Pedraforca thrust sheets emplacement (Cruset et al., 2020), and creation of vein networks along the South Pyrenean Frontal Thrust (Hoareau et al., 2021). U-Pb data on absolute timing of deformation in the northern front of the Pyrenean orogen are still scarce (Parizot et al., 2022), highlighting the need for further investigations to establish precise temporal constraints.

**Project administration:** Yves Missenard
**Supervision:** Yves Missenard
**Validation:** Agathe Jullien-Sicre, Yves Missenard, Thomas Blaise, Romain Augier
**Visualization:** Agathe Jullien-Sicre, Yves Missenard, Thomas Blaise
**Writing – original draft:** Agathe Jullien-Sicre
**Writing – review & editing:** Yves Missenard, Thomas Blaise, Romain Augier, Oriane Parizot, Frédéric Haurine

The intraplate domain shows significant deformation, hundreds of kilometers away from the orogen, due to the effect of far-field deformation. This deformation is expressed through lithospheric buckling (Cloetingh et al., 1999; Gerbault et al., 1999; Sokoutis et al., 2005), reactivation of crustal scale inherited structures (Ziegler et al., 1995) and creation of newly formed small-scale brittle structures such as faults, joints or tension gashes (Bergerat, 1987; Lacombe & Obert, 2000; Navabpour et al., 2017). U-Pb geochronology on syn-kinematic calcite has also opened the way to assign ages to the formation of small-scale brittle structures (Blaise et al., 2022), regional folding (Connolly et al., 2024; Parrish et al., 2018), and inherited structures (Monchal et al., 2023; Parizot et al., 2022) in the Eurasian plate, and draw connections with major geodynamic events that took place at plate boundaries. Precise dating of this structures reveals that the stress induced by Pyrenean orogeny was recorded in a variety of tectonic objects and throughout the western European intraplate domain. While the eastern Paris Basin seems to record continuous deformation, generated by the Pyrenean orogen, from ca. 48 to 35 Ma (Blaise et al., 2022), in the Hampshire basin (Parrish et al., 2018) and in Ireland (Monchal et al., 2023) folding and fold reactivation were associated with a N-S shortening over a shorter period of time between ca. 35 to 31 Ma.

The chronology of interactions among the pro-foreland, retro-foreland, and intraplate domains is still not fully constrained. It is unclear whether these domains respond to Africa, Iberia, Eurasia convergence synchronously. The timing of deformation between the pro-foreland and retro-foreland remains relatively unknown, as does the response of the intraplate domain to deformation at plate boundaries. While the northern Pyrenean foreland has been the focus of numerous studies to comprehend the structure, the thermal history, the structural inheritance and the timing of deformation (Choukroune & Delair, 1976; Clerc et al., 2015; Lagabrielle et al., 2010; Puigdefàbregas & Souquet, 1986), inadequate outcropping conditions and a complex stratigraphic record pose challenges in establishing a precise chronology of deformation. The objective of this study is to clarify the timing of deformation in the Eastern Pyrenees within the North and Sub-Pyrenean Zone. This refinement is achieved through the inversion of fault-slip data coupled with syn-kinematic calcite, along with the in-situ calcite U-Pb geochronology. Our newly acquired geochronological data are compiled with other published calcite U-Pb ages to compare the timing of deformation in both forelands, as well as in the Western European intraplate domain. We propose a deformation timeline that highlights the interactions between plate interiors and plate boundaries throughout the complete Pyrenean orogenic and post-orogenic history, demonstrating the synchronicity of deformation between the plate boundaries and the intraplate domain of the overriding plate.

## 2. Geological Context

### 2.1. Geodynamic Framework

The Pyrenean belt belongs to the Alpine orogenic system that runs from east to west across southern Europe. The belt results from the inversion of Early-Cretaceous rift basins carrying evidences of syn-rift high-temperature and low-pressure (HT-LP) metamorphism and mantle exhumation (Canérot, 2017; Choukroune, 1989; Lagabrielle & Bodinier, 2008; Mouthereau et al., 2014; Teixell et al., 2018; Vergés et al., 2002). Shortening results from the convergence of the Iberian Plate with Europe from the Late Santonian to until the Oligocene and early Miocene (Mouthereau et al., 2014; Teixell et al., 2018; Vergés et al., 1995) in the overall, still active convergence between Africa and Eurasian plates (Ford et al., 2022; Jolivet et al., 2021; Platt et al., 1989; Rosenbaum et al., 2002).

The Pyrenean belt appears as a quite symmetrical collisional orogen with two distinctive foreland systems. The down going Iberian plate bears the Pyrenean pro-foreland and the overriding European plate, the retro-foreland (Choukroune, 1976; Ford et al., 2016; Grool et al., 2018; Teixell et al., 2018). The Axial Zone corresponds to the central part of the mountain range structured by thick Precambrian and Paleozoic thrust sheets (Laumonier et al., 2010; Vissers, 1992). The retro-foreland extended over ca.300 km further east in Languedoc and southern Provence (Bestani et al., 2015; Lacombe & Jolivet, 2005). However, both the Pro-foreland and the Axial Zone end abruptly toward the east against the Golf du Lion passive margin (Jolivet et al., 2020). There, the Pyrenean belt experienced a local, yet complete post-orogenic collapse related to the retreat of the Mediterranean slabs started at ca. 35–30 Ma (Séranne et al., 2021).



19449194, 2025, 2, Downloaded from https://agupubs.onlinelibrary.wiley.com/doi/10.1029/2024TC008634 by Portail BibCNRS INSU, Wiley Online Library on [03/03/2025]. See the Terms and Conditions (https://onlinelibrary.wiley.com/terms-and-conditions) on Wiley Online Library for rules of use; OA articles are governed by the applicable Creative Commons License

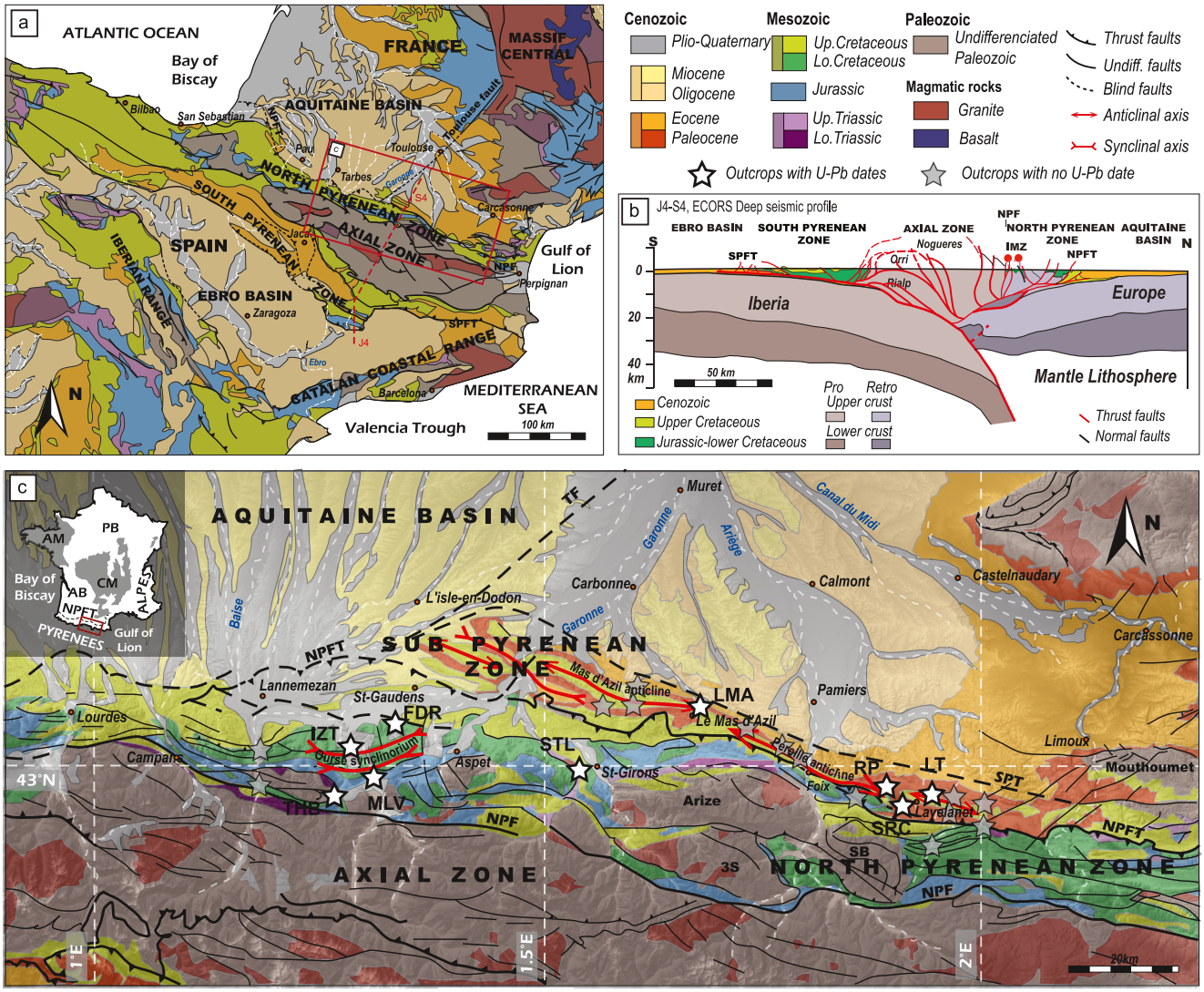


**Figure 1.** (a) Structural sketch of the Pyrenean belt and adjacent areas, modified after the 1/1 000 000 BRGM geological map of France. The red dotted line indicates the ECORS profile trace shown in panel (b) and the red square matches the location of the studied area shown in panel (c). (b) Interpretation of the ECORS J4-S4 Pyrenees deep seismic section showing the asymmetry of the orogenic wedge and major structural zones; modified after Ford et al. (2022). (c) Structural map of the study area, modified after the 1/1 000 000 and 1/50 000 BRGM geological maps of France. PB, Paris Basin; AM, Armorican Massif; CM, Central Massif; AB, Aquitaine Basin White stars locate the sampling areas, from east to west: LT, SRC, RP, LMA, STL, FDR, MLV, IZT, and THB. NPFT, North Pyrenean Frontal Thrust; SPT, Sub Pyrenean Thrust; NPF, North Pyrenean Fault; SPFT, South Pyrenean Frontal Thrust; 3S, Trois Seigneurs massif; SB, Saint Barthelemy massif.

## 2.2. Structural Framework

### 2.2.1. Pro-Foreland Basin

The Pyrenean pro-foreland basin comprises the South Pyrenean Zone and the Ebro Basin. The South Pyrenean Zone is a prominent fold-and-thrust belt, delineated to the north by the Axial Zone and to the south by the South Pyrenean Frontal Thrust. This unit overrides the mildly deformed Ebro Basin (Figure 1a). The thickness of evaporite deposits significantly influences the deformation style within the basin. The eastern part, where Upper Triassic evaporites are often absent, is structured by a classical flexural basin (Vergés et al., 1995, 2002). The South Central Pyrenean Unit is composed of southward stacked thrust sheets rooted in the thick Upper Triassic salt (Cruset et al., 2020; Ford et al., 2022; Muñoz-López et al., 2022; Teixell et al., 2018) (Figure 1b). Westward, in the Jaca basin, little to no evaporites are found (Ford et al., 2022; Labaume et al., 1985; Labaume & Teixell, 2018), the unit is formed of several WNW-ESE trending thrusts cross-cutting anticline folds (Arenas et al., 2001; Hoareau



19449194, 2025, 2, Downloaded from https://agupubs.onlinelibrary.wiley.com/doi/10.1029/2024TC008634 by Portail BibCNRS INSU, Wiley Online Library on [03/03/2025]. See the Terms and Conditions (https://onlinelibrary.wiley.com/terms-and-conditions) on Wiley Online Library for rules of use; OA articles are governed by the applicable Creative Commons License

et al., 2021). Finally, in the westernmost part of the Jaca Basin, thick but narrow syn-orogenic evaporite deposits are confined by thrusts north and south of the system (Ford et al., 2022; Larrasoaña et al., 2003).

#### 2.2.2. Retro-Foreland Basin

The Aquitaine Basin reaches 300 km in width at its largest. It is delineated to the north by the French Central Massif (Figure 1). East of the Toulouse fault, delineating boundaries is more challenging due to the Cenozoic uplift of the Massif Central (Barbarand et al., 2013). The basin infill is relatively well preserved from the Mesozoic to the Cenozoic (Ford et al., 2022; Rougier et al., 2016). Our studied area is located east of the Toulouse fault where basin infill overlies unconformably the Variscan basement (Ducoux et al., 2022; Serrano et al., 2006). Further south, the folded (e.g., the WNW-ESE trending Lavelanet anticline or the Mas-d'Azil anticline (Figure 1c)) and faulted pre- and syn-orogenic sediments constitute the Sub Pyrenean Zone (Rougier et al., 2016). It is bounded by the blind Sub Pyrenean Frontal Thrust, to the north, and the North Pyrenean Frontal Thrust, to the south (Figure 1c). Between the Sub Pyrenean Zone and the Axial Zone is the North Pyrenean Zone. This narrow north-verging belt is composed of inverted Mesozoic rift basins (e.g., the Camarade basin (Baby et al., 1988)) and inverted Paleozoic basement massifs (e.g., the Saint Barthelemy Massif, the 3 Seigneurs massif or the Arize Massif (Vergés et al., 1995)). It also encompasses the Internal Metamorphic Zone, the product of Upper Cretaceous high temperature metamorphism (Ducoux et al., 2022; Golberg & Leyreloup, 1990). Eventually, it is circumscribed to the south by the steep North Pyrenean Fault, considered as the boundary between the Iberian and the European plate (Figure 1) (Muñoz, 1992).

Mesozoic sedimentation in the eastern and central part of the Pyrenees begins with the Trias Keuper evaporites. The formations of dolomites and Jurassic limestones (Bilotte et al., 1988), as well as the Berriasian-Barremian limestones, correspond to a littoral environment, forming the pre-rift units (Bilotte, 1978; Grool et al., 2018; Rougier et al., 2016). The syn-rift unit (Debroas, 1990; Grool et al., 2018; Souquet et al., 1985), are Aptian-lower Cenomanian deep marine shaly limestones. From Cenomanian to Santonian, platform limestones were deposited, followed by deep-water marls, forming the post-rift sediments (Debroas, 1990; Souquet et al., 1985). The early syn-orogenic sequence are lower Campanian to middle Maastrichtian deep marine shales and fluvial/deltaic sands (Bilotte et al., 1988; Grool et al., 2018; Rougier et al., 2016). They deposit during the basin first subsidence phase and are mainly enclosed in the Sub Pyrenean Zone. From the middle Maastrichtian, red mudstones, sandstones, and conglomerates rest unconformably above (Bilotte et al., 1988; Grool et al., 2018). These sediments are the product of the exhumation and erosion of the Pyrenees. In the upper sequence, the marine Thanetian sometimes interfingers with the continental series. The early marine Ypresian spans the entire basin (Bilotte et al., 1988; Cavaillé et al., 1975; Tambareau et al., 1995). From the late Ypresian, sedimentation mainly consists of fluvial sandstones and conglomerates, which extends across the foreland (Bilotte et al., 1988; Grool et al., 2018). The upper section, likely to be Miocene, lacks precise dating.

#### 2.2.3. The Gulf of Lion

The Gulf of Lion forms the northwestern rifted continental margin of the Liguro-Provençal basin, bounded on the proximal side by the Cévennes fault. The Nîmes fault marks the northeastern boundary of a low-angle faulted basement domain which extends mainly offshore. The landward part of the margin is a thin-skinned extensional domain characterized by half grabens (Benedicto et al., 1996; Jolivet et al., 2020; Séranne, 1999). These extensional structures are oriented mainly NE-SW, overprinting the Pyrenean thrust and fold belt (Séranne, 1999). Séranne et al. (2021) synthesizes the sedimentary sequence marking the transition from Pyrenean compression to Miocene rifting in the Languedoc region. The Paleocene to lower Eocene deposits consists of fluvial marls, associated with syn-tectonic breccias from the early Pyrenean compression, reworking Jurassic materials near the Montpellier thrust. Above these, massive Lutetian limestones form a continuous folded unit linked to later stages of Pyrenean compression. These limestones are overlaid by a Bartonian unit of lacustrine to shallow marine marly facies. The uppermost Paleogene deposits are Priabonian fluvial sediments, composed of conglomerates, sandstones, and marls, derived from both distant Pyrenean sources and local Mesozoic carbonates, resting unconformably on the folded Lutetian to Bartonian units. This Priabonian unit is described as an intermediate between the previously mentioned syn-orogenic deposits and the syn-rift Rupelian alluvial breccias and marls.



19449194, 2025, 2, Downloaded from https://agupubs.onlinelibrary.wiley.com/doi/10.1029/2024TC008634 by Portail BibCNRS INSU, Wiley Online Library on [03/03/2025]. See the Terms and Conditions (https://onlinelibrary.wiley.com/terms-and-conditions) on Wiley Online Library for rules of use; OA articles are governed by the applicable Creative Commons License

### 2.3. Existing Time-Constraints on the Main Deformation Events

During Aptian to early Cenomanian, rift systems spanned along the Iberia-Europe zone, broadening to the west down to the oceanic domain of the Bay of Biscay with a sinistral strike-slip movement (Choukroune & Mattauer, 1978; Ford et al., 2016; Jolivet et al., 2021; Mouthereau et al., 2014). However the relative motion between Iberian and European plates is still debated in light of the magnetic quiescence during Aptian to Santonian (Angrand et al., 2018; Jolivet et al., 2021).

The onset of convergence, accompanied by the inception of the subduction of hyper-extended domain and the initiation of flexural basin are estimated to have begun at ca. 83–84 Ma, in the North Pyrenean foreland (Mouthereau et al., 2014; Teixell et al., 2018), or even earlier, during the Coniacian and early Santonian (Andrieu et al., 2021), according to sedimentological approaches. The onset of shortening in the Southern Pyrenees seems harder to constrain, the preserved subsidence signal is not clear and strata dating uncertain from Maastrichtian to Paleocene (Grool et al., 2018). Some authors place this onset ca. 72 Ma in the Pedraforca thrust sheet (Puigdefàbregas & Souquet, 1986), and others in the late Santonian, ca. 84 Ma (McClay et al., 2004; Saura et al., 2016; Teixell, 1996). In those early stages, convergence is accommodated by the subduction of the Iberian margin in the south and thrusting along the North Pyrenean Frontal Thrust in the north (Grool et al., 2018). The orogenic phase begins during Campanian time, ca when both necking zones collide (Christophoul et al., 2003; Jolivet et al., 2021; Mouthereau et al., 2014). The main thrusts were then formed to the north and south of the Pyrenees. Folding occurs due to N-S oriented compressive stress, which is combined with a slight left-lateral strike-slip shearing parallel to the North Pyrenean Fault (Cruset et al., 2020; Grool et al., 2018). Additionally, an increase in subsidence is recorded during this period (Ford et al., 2022; Grool et al., 2018).

From the early Maastrichtian to the Paleocene-Eocene boundary, little to no convergence is recorded (Macchiavelli et al., 2017), no fault activity is documented during Paleocene time and very slight subsidence is observed, associated with thin continental deposits (Grool et al., 2018).

The main orogenic phase spans from Thanetian to the late Chattian (ca. 59 to 23 Ma) (Christophoul et al., 2003; Grool et al., 2018; Macchiavelli et al., 2017; Parizot et al., 2021; Sainz & Faccenna, 2001; Vergés et al., 1995). In the Northern Pyrenees, continental conglomerates deposition in the retro-foreland basin spanned from the middle Ypresian to the early Oligocene, reflecting slow tectonic subsidence (Ford et al., 2022; Grool et al., 2018; Rougier et al., 2016) and the paroxysmal phase (Al Reda et al., 2021). Main structures as E-W trending regional folds and thick-skin accretion are the result of pure N-S oriented compressive stress (Christophoul et al., 2003). The most recent phase of deformation is expressed by the slight folding of the Priabonian upper unit of the Carcassonne group (Grool et al., 2018). In the Southern Pyrenees, from the early Eocene, the thrust front propagated rapidly with the progressive south-directed stacking of piggyback thrust sheets until the late Oligocene (ca. 23 Ma) (Cruset et al., 2020; Grool et al., 2018).

In the Mediterranean region, subduction dynamics underwent a significant change at 35-30 Ma (Jolivet & Faccenna, 2000). The African slab subducting beneath Europe began to retreat, leading to the counter-clockwise rotation of the Sardinia-Corsica continental block and the opening of the Liguro-Provençal basin (Jolivet et al., 2020; Séranne, 1999). Séranne et al. (2021) demonstrates that rifting began during Rupelian time (34–28 Ma) at ca. 32–30 Ma, causing a fast dismantling of the easternmost part of the Pyrenean belt, marking the end of the significant shortening deformation. However, in the western Pyrenees (on the northern side), the end of shortening occurred during Oligocene time (ca. 34 to 23 Ma), according to the incomplete sedimentation record due to a regional uplift of the French Central Massif (Ford et al., 2016; Grool et al., 2018; Jolivet et al., 2021; Macchiavelli et al., 2017). Furthermore, plate reconstructions set the end of Iberia-Europe convergence at 23 Ma (Ford et al., 2022; Macchiavelli et al., 2017). These observations highlight a diachronism in the end of the orogeny between the western and eastern parts of the belt.

Parizot et al. (2021) documented recently a renewal of activity along the North Pyrenean Frontal Thrust during the early/middle Miocene. Moreover, in the Jaca basin, compressional veins in the Santo Domingo anticline were dated, using U-Pb carbonate geochronology, by Hoareau et al. (2021), giving a crystallization age of ca.17 Ma. Until then, the timing of this fold development was dated between Chattian and Aquitanian times (ca. 28–20 Ma) by magnetostratigraphy (Oliva-Urcia et al., 2019). In the south foreland basin of the orogen, the youngest deformed sediments are Rupelian continental formations indicating that deformation occurred until a minimum age of ca. 28 Ma (Ford et al., 2022; Grool et al., 2018; Macchiavelli et al., 2017). On the southern side of the



19449194, 2025, 2, Downloaded from https://agupubs.onlinelibrary.wiley.com/doi/10.1029/2024TC008634 by Portail BibCNRS INSU, Wiley Online Library on [03/03/2025]. See the Terms and Conditions (https://onlinelibrary.wiley.com/terms-and-conditions) on Wiley Online Library for rules of use; OA articles are governed by the applicable Creative Commons License

19449194, 2025, 2, Downloaded from https://agupubs.onlinelibrary.wiley.com/doi/10.1029/2024TC008634 by Portail BibCNRS INSU, Wiley Online Library on [03/03/2025]. See the Terms and Conditions (https://onlinelibrary.wiley.com/terms-and-conditions) on Wiley Online Library for rules of use; OA articles are governed by the applicable Creative Commons License

Pyrenean belt, U-Pb dating of syn-faulting calcite, in the Pedraforca and Cadi thrust sheets, recorded normal fault activity between ca. 30 to 12 Ma (Cruset et al., 2020). Cruset et al. (2020) suggests that these normal faults are a consequence of stacking and exhumation of Pyrenees hinterland (Fillon et al., 2013; Rushlow et al., 2013).

## 3. Materials and Methods

### 3.1. Sampling Strategy

Constraining the timing of shortening brittle deformation hinges on our capacity to link calcite growth to fault displacement or fold development as recently described (Blaise et al., 2022; Connolly et al., 2024; Cruset et al., 2020; Hoareau et al., 2021; Monchal et al., 2023; Parizot et al., 2020, 2021, 2022; Parrish et al., 2018; Roberts et al., 2021). Ensuring such a robust tectonic control requires a careful microstructural study including primarily detailed field inspections and inversion of fault slip data. Sampling focused on syn-kinematic fault-related calcite. Each sample consists of a single family of striations, hence a single deformation event. The caution regarding our sampling strategy is taken to avoid multiple fluid circulation, meaning several episodes of dissolution and recrystallization during which the isotopic system may be reopened, adding difficulties to the interpretation of geochronological data. From Lavelanet to Lannemezan, east to west, in the North Pyrenean Zone and the Sub Pyrenean Zone (Figure 1), 57 synkinematic fault-related calcite were collected on upper Oxfordian to lower Thanetian limestones, from natural outcrops and quarries. Fault planes (strike-dip angle + direction of dip) and slickenfiber orientation (pitch angle + direction of dip) were measured on each sample site. Palaeostress orientations were obtained using WinTensor© software (Delvaux & Sperner, 2003) for fault-slip data (see also details in Angelier and Mechler (1977)). The reduced palaeostress tensor consists in the identification of the orientation of the three principal stress axes and a ratio reflecting the relative magnitude of principal stress axes (axial ratio of stress ellipsoid). Determination of the palaeostress axes were complemented by the analysis of other accompanying brittle structures such as folds, joints, tension gashes or bedding-parallel planes (Doblas, 1998; Hancock, 1985).

### 3.2. Sample Preparation and Imaging

To gather the most accurate tectonic control, calcite samples that consist in slickenfibers developed along the fault planes were all cut in the plane that contains striations, along the X-Z structural plane. Calcite samples were then mounted in epoxy as series of 3–6 calcite fragments of ca. 0.5–2 $cm^2$-sized polished surfaces. Due to their relative opacity, calcite samples were first observed under the binocular microscope in reflected light. Samples were imaged using cathodoluminescence (CL) to identify zoning or heterogeneous phases that might exist within the sample. Providing useful information on calcite growth history particularly in relation to movements on fault planes, CL were performed on all samples at GEOPS (University of Paris-Saclay). CL imaging (Cathodyne, NewTec Scientific, France) was performed using the following parameters: between 10 and 12 keV and 150–200 mA. Since the distribution of U and Pb within samples can be highly heterogeneous and independent of the phases, Laser-Ablation Inductively Coupled Mass Spectrometer (LA-ICP-MS) isotopic mapping was used on samples that were difficult to characterize by CL imaging only. Analysis were conducted at the ISTO, (University of Orléans), using an 8900 quadrupole ICP-MS (Agilent, Santa Clara, CA, USA) coupled to a 193 nm ArF Resolution SE laser ablation system (Applied Spectra, West Sacramento, CA, USA). Samples were ablated along 35 linear traverses of 11 mm length typically corresponding to ~2 min of data acquisition per line. Traverses were arranged without overlaps or gaps between successive lines with an 80 µm square spot allowing the imaging or an overall ca. 3 mm width. Traverses were undertaken using a fluence of typically 5 $J/cm^2$, repetition rates of 20 Hz, and continuous stage movement rates of 160 µm/s.

### 3.3. In Situ Calcite U-Pb Geochronology

U-Pb geochronology on syn-kinematic calcite were carried out on a High-Resolution Inductively Coupled Mass Spectrometer (HR-ICP-MS) (Element XR from Thermo Scientific™, Waltham, MA, USA) coupled with a 193 nm ArF laser ablation system (Analyte Excite Excimer from Teledyne, Thousand Oaks, CA, USA) at the Geosciences Paris-Saclay (GEOPS) laboratory at Paris-Saclay university (Orsay, France) following the procedure described in Blaise et al. (2022). Glass reference material (RM) NIST614 was used to correct $^{207}Pb/^{206}Pb$ fractionation, while WC-1 RM (Roberts et al., 2017; Woodhead et al., 2016) was used to correct $^{238}U/^{206}Pb$ ratios using the 254.4 ± 6.4 Ma intercept age obtained by isotope dilution - thermal ionization mass spectrometry (ID-TIMS). To

19449194, 2025, 2, Downloaded from https://agupubs.onlinelibrary.wiley.com/doi/10.1029/2024TC008634 by Portail BibCNRS INSU, Wiley Online Library on [03/03/2025]. See the Terms and Conditions (https://onlinelibrary.wiley.com/terms-and-conditions) on Wiley Online Library for rules of use; OA articles are governed by the applicable Creative Commons License

ensure accuracy of these corrections, secondary calcite RMs were then analyzed including the JT calcite vein, dated at 13.7 ± 0.3 Ma by ID-TIMS (Guillong et al., 2020), the AUG-B6 calcite breccia, dated at 43.0 ± 1.0 Ma by LA-ICP-MS (Pagel et al., 2018) and the RA138 botryoidal cement dated at 321.99 ± 0.6 Ma by ID-TIMS (Guillong et al., 2024). To rule out unsuitable samples for U-Pb geochronology and/or suitable areas in a crystal, 10 ablation spots were analyzed (prescan) prior to final U-Pb data acquisition. To reduce potential surface contamination each spot was pre-ablated with a 155 µm diameter spot, a frequency of 8 Hz and a fluence of 2 J/cm$^2$ for 5 s. The ablation parameters used for data acquisition were a laser beam diameter of 150 µm, and a frequency of 8 Hz coupled with a fluence of 4 J/cm$^2$. Analysis time included 30 s of background measurement, firing laser for 30 s followed by 30 s of washout. 30 to 40 ablation spots were routinely analyzed on each sample. Data was reduced using Iolite© (Lawson et al., 2018; Paton et al., 2011). Reduced data was plotted in a Terra-Wasserburg $^{238}U/^{206}Pb$ versus $^{207}Pb/^{206}Pb$ using the online version of IsoplotR© (Vermeesch, 2018). In each Terra-Wasserburg graph, two age uncertainties are given. The first uncertainty does not take into account error propagation, except the errors related to the decay constants of $^{235}U$ and $^{238}U$ using IsoplotR©. A second date uncertainty is given, by propagating the systematic uncertainty of primary reference material WC-1 age (2.6%), and the two sigma standard errors of the $^{207}Pb/^{206}Pb$ and $^{206}Pb/^{238}U$ of the corresponding analytical session and a 2% error to take into account the estimated long term excess variance, by quadratic addition. The detailed metadata associated with calcite U-Pb geochronology are given in Supporting Information S1.

## 4. Results

### 4.1. Petrography of the Calcite Samples and Selection of the Laser Ablation Zone(s)

Petrographic observations, coupled with prescan results, were used to identify any zoning or complex textures within the sample. As shown in Figure 2 the sample FDR3 representing a single shearing event in reflected light (Figure 2a) exhibits episodes of shearing/dilation in cathodoluminescence (Figure 2b). Most samples present rather homogeneous luminescence, as LMA3 (Figures 2a and 2b) preventing from understanding the calcite growth history. LA-ICP-MS isotopic mapping was employed to identify the areas within the crystal with suitable $^{238}U$, $^{207}Pb$ and $^{206}Pb$ signal intensities for U-Pb dating, as the distribution of U and Pb in the crystal is complex and not necessarily linked to the different phases of fluid circulation. The LA-ICP-MS mapping of the FDR3 sample (Figure 2c) shows that the distribution of lead is not correlated with that of uranium within the sample. The distribution of uranium is closely correlated with the crack-seal patterns (Bons et al., 2012; Vergely & Xu, 1988), whereas the distribution of lead is much less zoned. All samples are syn-kinematic slickenfiber calcite showing various textures such as granular texture (e.g., sample LMA3, Figure 2b), or fibrous texture (e.g., sample FDR3, Figure 2b) in CL microscopy and isotopic mapping. Some samples display evidence of multiple phases of fluid circulation, such as cataclastic texture, or crackseal figures (e.g., sample LMA3, Figure 2). Under CL crystals are weakly luminescent going from brown to orange tones. Apart from MLV3, STL1 and FDR1 samples, no evidence of multi-phase syn-faulting calcite growth was observed. No dissolution evidence was observed. Petrographic illustrations of all samples are available in Supporting Information S1.

Following textural analysis of the samples, prescan aimed at targeting all phases within each sample. Out of 57 syn-kinematic slickenfiber calcite, only 21 (37%) were selected for in situ U-Pb dating after the prescan analysis. The remaining samples were judged unsuitable for U-Pb geochronology analysis due to either low uranium concentration, high common lead concentration, or both.

### 4.2. Structural Observations

Structural analysis of microstructures and the associated sampling were conducted on 23 sites in the North and Sub-Pyrenean Zone (Figure 1c). A total of 163 fault planes and syn-kinematic calcite were measured. All the tectonic structures observed during fieldwork were either reverse faults or strike-slip faults or bedding-parallel planes (Figure 3). No normal faults were observed. Reverse faults are broadly striking E-W, strike ranges from N60° to N130° and dip from 20° to 50°(Figure 3). Strike-slip faults are mainly sinistral, striking NW-SE, between N°110 and N°150 (Figure 3). Dextral faults are uncommon; they strike NNE-SSW. When found in the same location, sinistral and dextral faults crosscut each other in a conjugated system (Figure 3). Flexural-slip planes are very common in the fold-and-thrust belt and mainly encountered in the vertical limbs of anticlinal folds. They strike E-W, between N80° and N125°, in the same direction as fold axis (Figure 3). For tectonic inversion, only reverse and strike-slip planes were analyzed as a bulk population without division based on

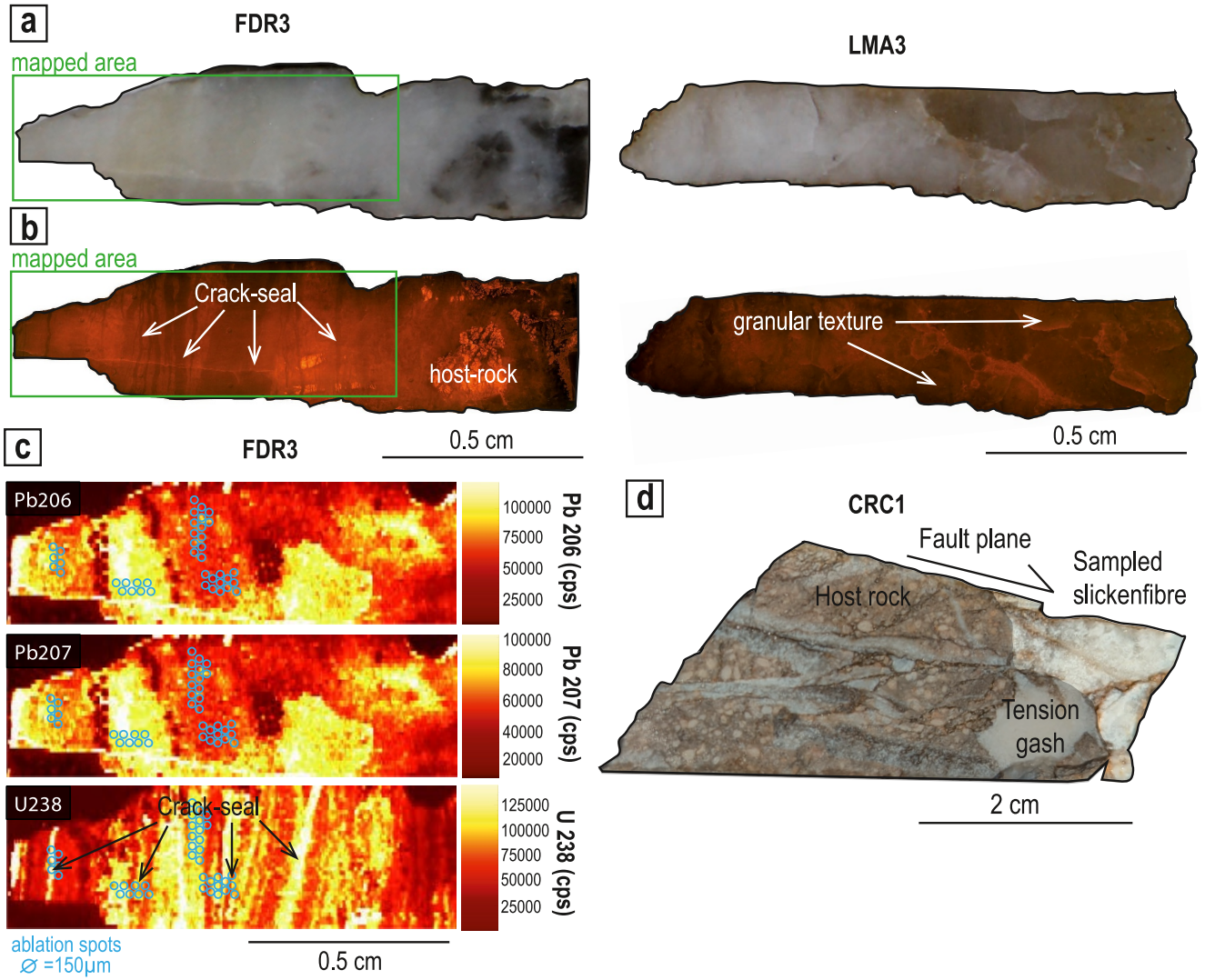


**Figure 2.** (a) Examples of petrographic observations on syn-kinematic calcite slickenfibers of granular (LMA3) or fibrous (FDR3) texture, (b) in cathodoluminescence. (c) Distribution of $^{238}U$, $^{207}Pb$ and $^{206}Pb$ isotopes within sample FDR3 (green inset). (d) Hand sample of slickenfiber and host-rock, oriented perpendicular to the fault plane and parallel to the slickenside.

location in the field, as measured flexural slip planes are not suitable for data inversion using the right-dihedral method (Angelier & Mechler, 1977). The results of data inversion are presented in a rose diagram of the direction of maximum stress ($\sigma 1$) orientation frequency (Figure 4). Microtectonic data from all sites result in a N-S shortening tendency (N150° < $\sigma 1$ < N210°) (Figure 4) coherent with E-W oriented flexural slip planes (N80°–N125°) (Figure 3). Among samples of slickenfiber calcite selected for U-Pb dating, 7 crystals are sampled on flexural-slip fault planes striking from N80° to N125° (LMA3, LMA4, FDR6, LT, IZT6 and CRC1) (S1), 7 on reverse fault planes, striking from N37° to N122° (Figure 3) (FDR1, FDR3, RP2, LT3, STL1, STL2 and STL4) (S1), 6 on dextral fault planes striking from N26° to N105° (FRD5, FDR7, IZT1, THB4, MLV1, and FDR4) (S1) and 1 on a sinistral fault plane striking N20° (MLV3) (Figure 2).

### 4.3. Calcite U-Pb Geochronology

The 23 U-Pb dates and the corresponding Terra-Wasserburg diagrams are reported in Figure 5. For each Terra-Wasserburg diagram data are well scattered along the Discordia line and the MSWD (Mean Squared Weighted Deviation) of each data set ranges between 0.41 and 3.1.



19449194, 2025, 2, Downloaded from https://agupubs.onlinelibrary.wiley.com/doi/10.1029/2024TC008634 by Portail BibCNRS INSU, Wiley Online Library on [03/03/2025]. See the Terms and Conditions (https://onlinelibrary.wiley.com/terms-and-conditions) on Wiley Online Library for rules of use; OA articles are governed by the applicable Creative Commons License

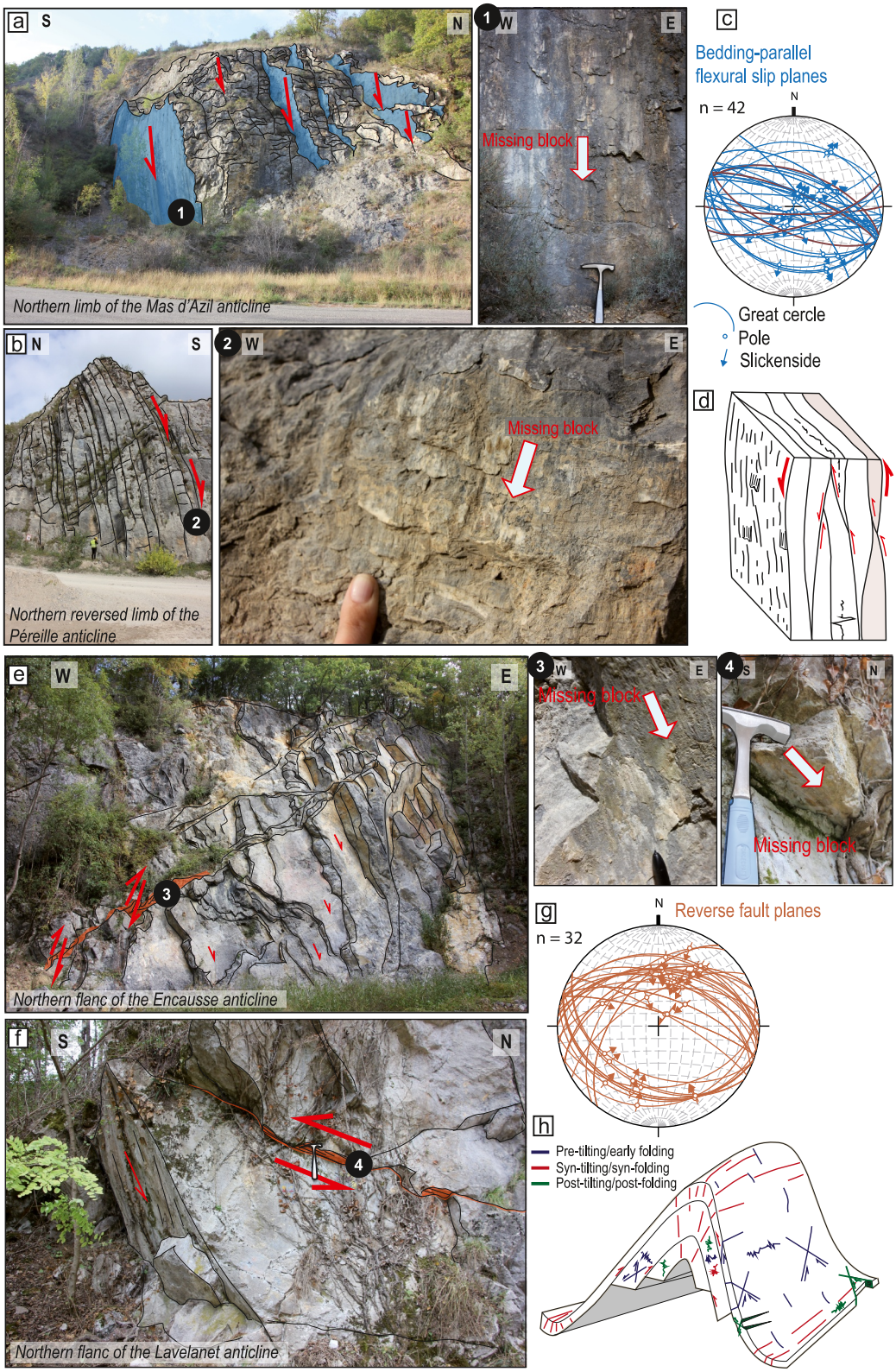


**Figure 3.** Examples of tectonic structures in the Ariège region. (a), (b) Pictures of flexural slip in anticlines, at different scales ((1, 2) Flexural slip slickenfibers). (c) Regional flexural slip planes in Wulf stereonet Lower hemisphere. (d) Diagram of flexural slip in folds modified after Choukroune (1976). (e), (f) Pictures of Late Stage Fold Tightening (LSFT) reverse faults, associated with syn-folding flexural slip, at different scales ((3, 4) reverse slickenfiber). (g) Regional reverse planes in Wulf lower hemisphere diagram. (h) Microstructures associated with folding modified from Lacombe et al. (2021). (i), (j) Pictures of strike-slip fault planes and associated slickenfibers (5, 6). (k) Regional strike-slip planes in Wulf lower hemisphere diagram.



19449194, 2025, 2, Downloaded from https://agupubs.onlinelibrary.wiley.com/doi/10.1029/2024TC008634 by Portail BibCNRS INSU, Wiley Online Library on [03/03/2025]. See the Terms and Conditions (https://onlinelibrary.wiley.com/terms-and-conditions) on Wiley Online Library for rules of use; OA articles are governed by the applicable Creative Commons License

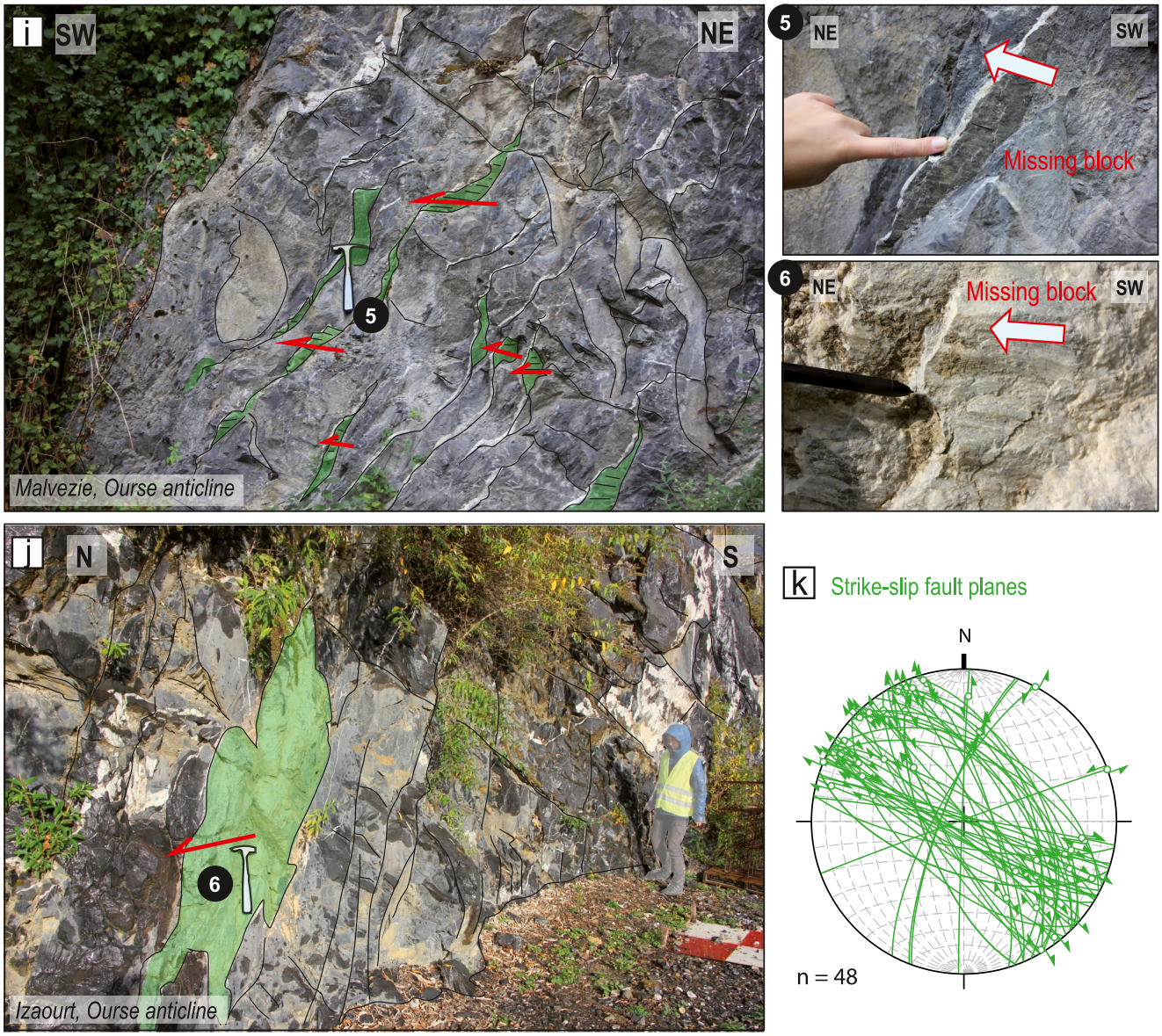


**Figure 3.** (Continued)

Two age groups are found. The first age group ranges from upper Ypresian to Rupelian, associated with syn- and late folding mesostructures (Figure 2h). The 17 obtained ages are between 30.8 ± 2.4 Ma (LT2) and 48.5 ± 3.1 Ma (STL4). These samples come from various locations (Figure 1) both on the Sub Pyrenean Zone and the North Pyrenean Zone on a hundred kilometers wide area. In STL1 brecciated texture (S1), both phases were suitable for U-Pb dating, yet the acquired dates failed to differentiate between these two crystallization events, as they produced a similar age of 36.0 ± 2 Ma (Figure 5). Among these samples, a cluster of age could be isolated from the rest of the data set, the samples RP2 (48.0 ± 2.4 Ma), STL3 (47.8 ± 1.9 Ma), LT1 (47.5 ± 8.9 Ma) and STL4 (48.5 ± 3.1 Ma) are all dated at ca. 48 Ma. The other samples are dated between 43.5 ± 1.5 Ma and 30.8 ± 2.4 Ma. Due to the uncertainties on some dates, it is difficult to identify another age cluster.

The second age group includes three calcite slickenfibers (IZT1, MLV3 and MLV1) sampled in the Ourse synclinorium in the North Pyrenean Zone, in two different locations, Izaourt and Malvezie (Figure 1). These samples have a Miocene age, Tortonian to Serravallian: 11.9 ± 0.7 Ma (MLV1) and 11.0 ± 1.8 Ma (MLV3), and



19449194, 2025, 2, Downloaded from https://agupubs.onlinelibrary.wiley.com/doi/10.1029/2024TC008634 by Portail BibCNRS INSU, Wiley Online Library on [03/03/2025]. See the Terms and Conditions (https://onlinelibrary.wiley.com/terms-and-conditions) on Wiley Online Library for rules of use; OA articles are governed by the applicable Creative Commons License

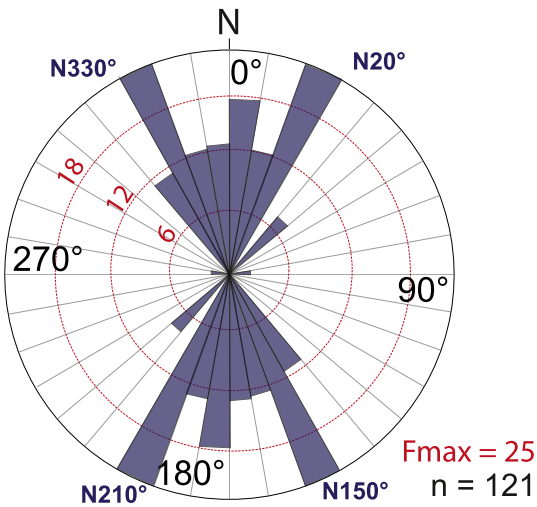


**Figure 4.** Rose diagram of the direction of maximum stress ($\sigma$1) orientation frequency of each reverse and strike-slip planes, analyzed as a bulk population without division based on location in the field.

Burdigalian: 16.3 ± 3.2 Ma (IZT6). MLV1 and MLV3 were sampled on conjugated strike-slip faults (Figures 2 and 5, Table 1). IZT6 is sampled on a flexural slip plane (Table 1). The MLV1 sample exhibits a heterogeneous texture and all phases were targeted by laser ablation, ablation spot location is available in S1. Three crystallization phases of different ages were identified (Figure 5, Table 1, and Table S1 in Supporting Information S1), only the most recent age, whose crystallization is identified to be associated with movement on the fault plane and the slickenside direction, is used for interpretation of geodynamic timeline in this study.

One of the samples (IZT1) was dated at 103 ± 26 Ma, an older age than the rest of the collected samples. The measured plan associated with IZT1 is a dextral fault, oriented N°114-89°N p64°E (Figure 5).

## 5. Discussion

### 5.1. Age of Brittle Structures Within the Pyrenean Retro-Foreland Basin

#### 5.1.1. Eocene-Oligocene Deformation: Tectonic Evolution of the Retro-Foreland

From late Ypresian to Rupelian times (ca. 56-28 Ma) brittle structures associated with folding events record a seemingly continuous deformation (oldest age: 48.5 ± 3.1 Ma, youngest age: 30.8 ± 2.4 Ma) (Figure 6). A N-S trending regional compressional stress regime (N150°-N210°) (Figure 4) is consistent with the major Pyrenean collisional event (Ford et al., 2022; Grool et al., 2018; Macchiavelli et al., 2017). Continental sedimentation stretches from the Ypresian to the Rupelian periods across the entire Aquitaine basin, indicating the main phase of deformation in the Retro-foreland basin (Al Reda et al., 2021) which is also consistent with the obtained data. The earlier signs of shortening are documented east of the studied area within the Lavelanet anticline (LT1: 47.5 ± 8.9 Ma) the Péreille anticline (RP2: 48.0 ± 2.4 Ma) and the Sourroque syncline (STL3: 47.8 ± 1.9 Ma, STL4: 48.5 ± 3.1 Ma) (Figure 6).

These results are consistent with a major hiatus in the sedimentary record in the northern Aquitaine Basin (Sztrákos et al., 2010) and the development of flexural basins in the southeastern part of the basin, such as the Corbières region (Christophoul et al., 2003), in this time frame. These tectono-sedimentary markers, coupled with the ages obtained in this study, indicate the resumption of the compressive regime in the northern Pyrenees and a NW directed transpressional movement of Iberia relative to Europe, from Ypresian to Lutetian times (Macchiavelli et al., 2017).

Obtained ages that span from 43.5 ± 1.5 Ma (CRC1) to 30.8 ± 2.4 Ma (LT2) (Figure 6) document fold growth as well as late stages of fold tightening across the eastern Pyrenees, while maximum exhumation is estimated ca. 40 Ma in the eastern axial zone by low-temperature thermochronology data (Bosch, Teixell, et al., 2016; Bosch, Van Den Driessche, et al., 2016; Labaume et al., 2016). Our data reveal that the retro-foreland basin, while it may be structured by in-sequence northward fault propagation (Christophoul et al., 2003), is reactivated along its compressive history, showing out-sequence stress propagation within folds (Figure 6).

#### 5.1.2. Miocene Deformation: A Renewal of Shortening?

The age group encompassing samples dated between ca. 16 and 11 Ma attests to Miocene tectonic activity in the North Pyrenean Zone. The oldest structure is dated at 16.3 ± 3.2 Ma (IZT6). This syn-kinematic calcite slickenfiber is associated with a flexural-slip fault plane (Figure 2a) with an azimuth oriented approximately N°110, compatible with a N-S $\sigma$1 stress regime. Conjugated strike-slip fault planes in the Ourse syncline (Figure 1c) also reveal Miocene deformation, with the dextral plane dated at 11.9 ± 0.7 Ma (MLV1) and the sinistral one at 11 ± 1.8 Ma (MLV3) (Figure 6). The strike-slip planes are either consistent with a N-S compression or a E-W extension.



19449194, 2025, 2, Downloaded from https://agupubs.onlinelibrary.wiley.com/doi/10.1029/2024TC008634 by Portail BibCNRS INSU, Wiley Online Library on [03/03/2025]. See the Terms and Conditions (https://onlinelibrary.wiley.com/terms-and-conditions) on Wiley Online Library for rules of use; OA articles are governed by the applicable Creative Commons License

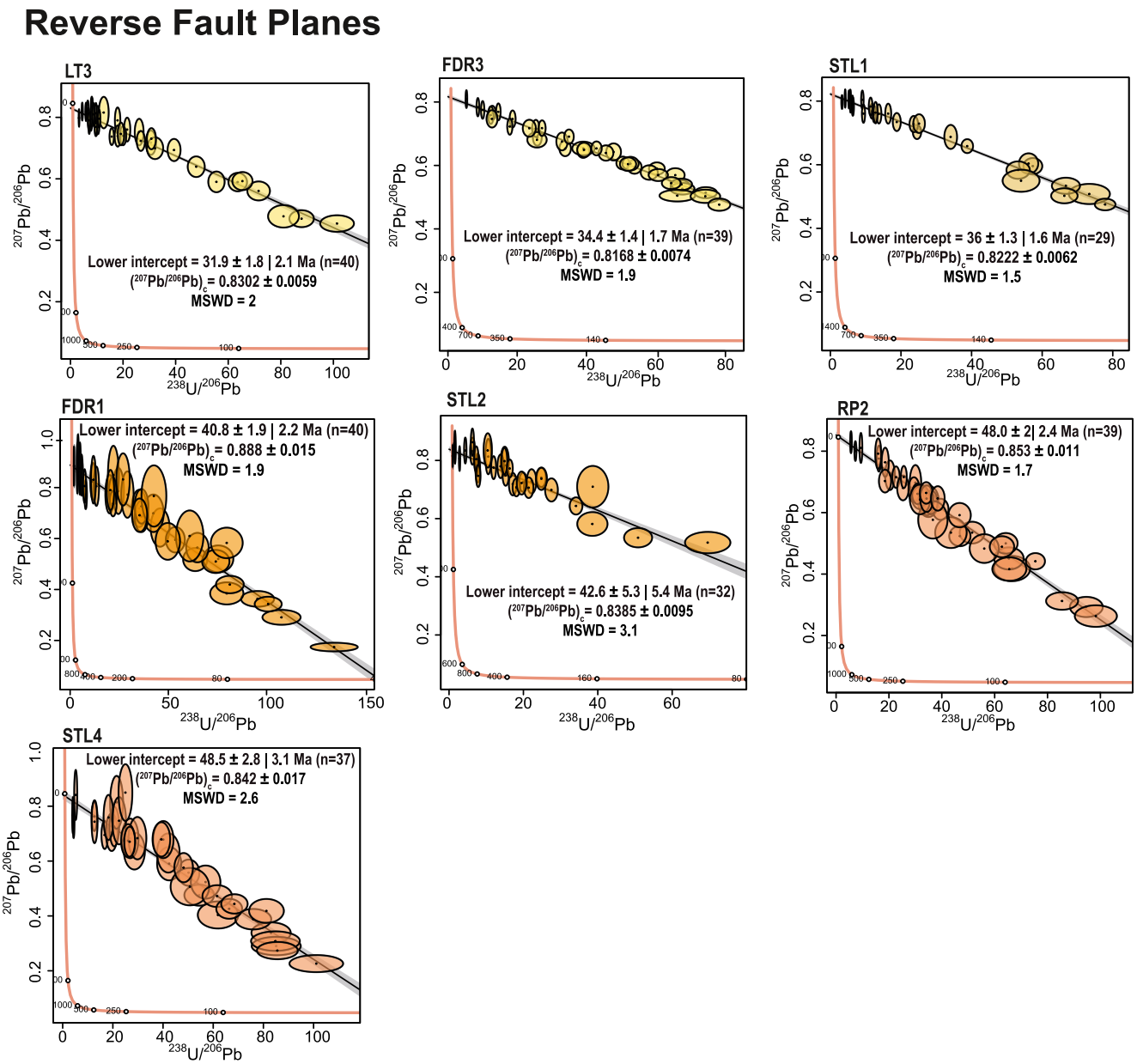


**Figure 5.** Terra-Wasserburg Discordia plots: U-Pb age of all samples, sorted by type, including fault planes and flexural slip. The color of the ellipses ranges from green, for the youngest ages to red for the older ones. Error ellipses of each spot and the error on the Terra-Wasserburg intercept age are 2$\sigma$. The first uncertainty does not take into account error propagation. A second date uncertainty is given, by propagating the systematic uncertainty of primary reference material WC-1 age, and the 2$\sigma$ standard errors of the $^{207}Pb/^{206}Pb$ and $^{206}Pb/^{238}U$ of the corresponding analytical session and a 2% error to take into account the long-term excess variance, by quadratic addition. MLV3 Terra-Wasserburg shows the three ages obtained in three different texture locations, difficult to identify in CL.

### 5.1.3. Cretaceous Deformation

The Cretaceous deformation episode recorded in the North Pyrenean Zone (sample IZT1) (Figure 7) is linked to an E-W trending dextral fault plane in a mid-Aptian lower Albian limestone. This sample covers a wide time frame due to significant uncertainties, 103 ± 26.1 Ma, from Barremian to Campanian. While extension is the main stress regime from Aptian to Cenomanian (Grool et al., 2018), early inversion of Mesozoic rifting is recorded from early Campanian (ca. 84 Ma) (Ford et al., 2022) as the early syn-orogenic sequence thickens, recording internal deformation, below the Lavelanet anticline (Grool et al., 2018). The central age suggests that this sample dates a fault plane formed during the aperture of the Pyrenean basins, specifically during Cenomanian, given the age of the



19449194, 2025, 2, Downloaded from https://agupubs.onlinelibrary.wiley.com/doi/10.1029/2024TC008634 by Portail BibCNRS INSU, Wiley Online Library on [03/03/2025]. See the Terms and Conditions (https://onlinelibrary.wiley.com/terms-and-conditions) on Wiley Online Library for rules of use; OA articles are governed by the applicable Creative Commons License

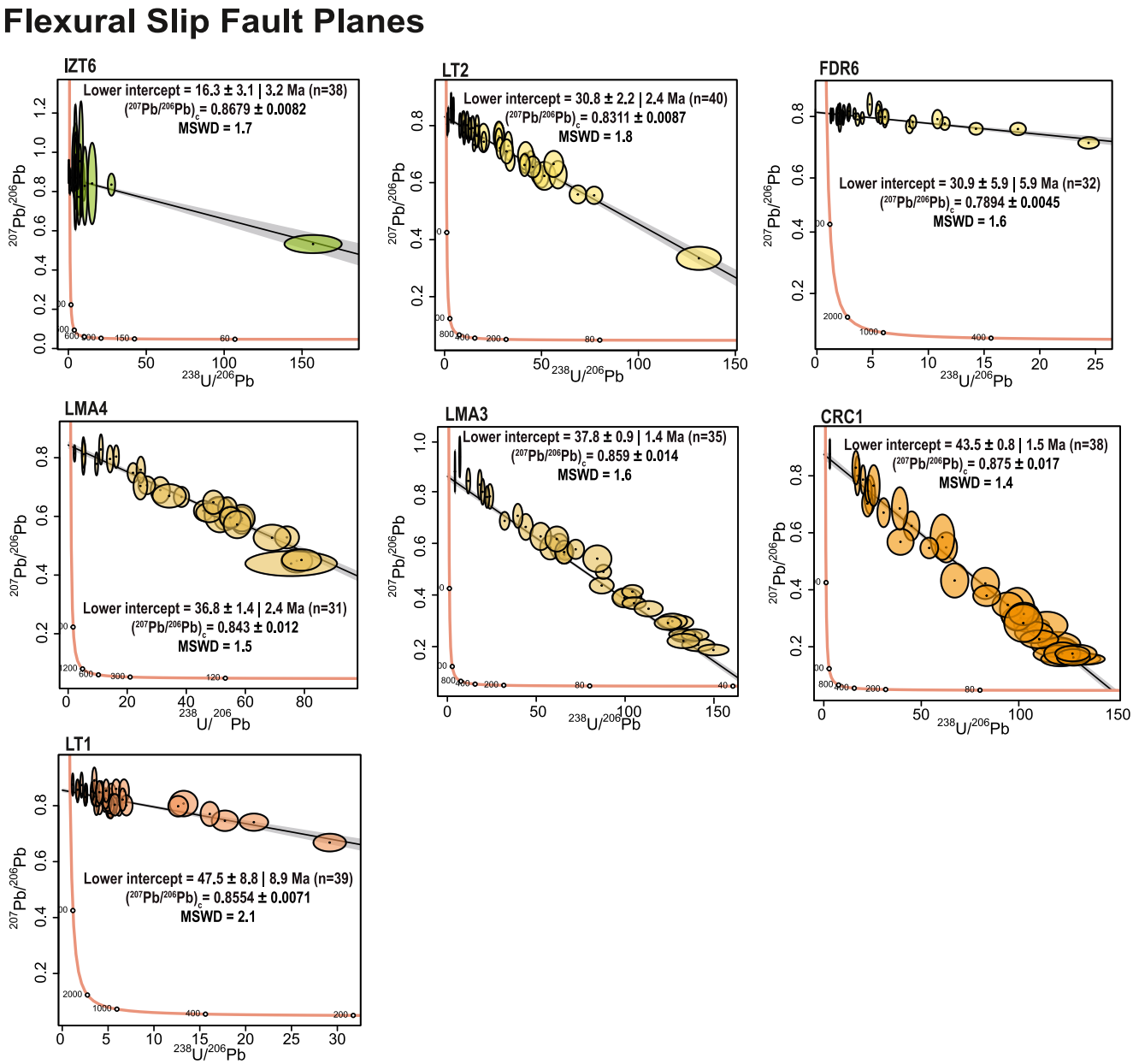


**Figure 5.** (Continued)

host rock. Inverting the fault plane data would help understand which geodynamic episode this deformation episode corresponds to, by giving a principal stress direction. However, the sample was taken from a massive limestone outcrop, and since bedding orientation cannot be confidently determined, structural data cannot be properly restored.

### 5.2. Syn and Post-Evolution of Asymmetrical Doubly Vergent Orogen as Recorded by Brittle Deformation in the Forelands

#### 5.2.1. Onset of Pyrenean Rift Inversion

Plate kinematic models place the onset of N-S convergence during Campanian (Angrand & Mouthereau, 2021; Macchiavelli et al., 2017; Rosenbaum et al., 2002), and many authors set the beginning of the Mesozoic Pyrenean



19449194, 2025, 2, Downloaded from https://agupubs.onlinelibrary.wiley.com/doi/10.1029/2024TC008634 by Portail BibCNRS INSU, Wiley Online Library on [03/03/2025]. See the Terms and Conditions (https://onlinelibrary.wiley.com/terms-and-conditions) on Wiley Online Library for rules of use; OA articles are governed by the applicable Creative Commons License

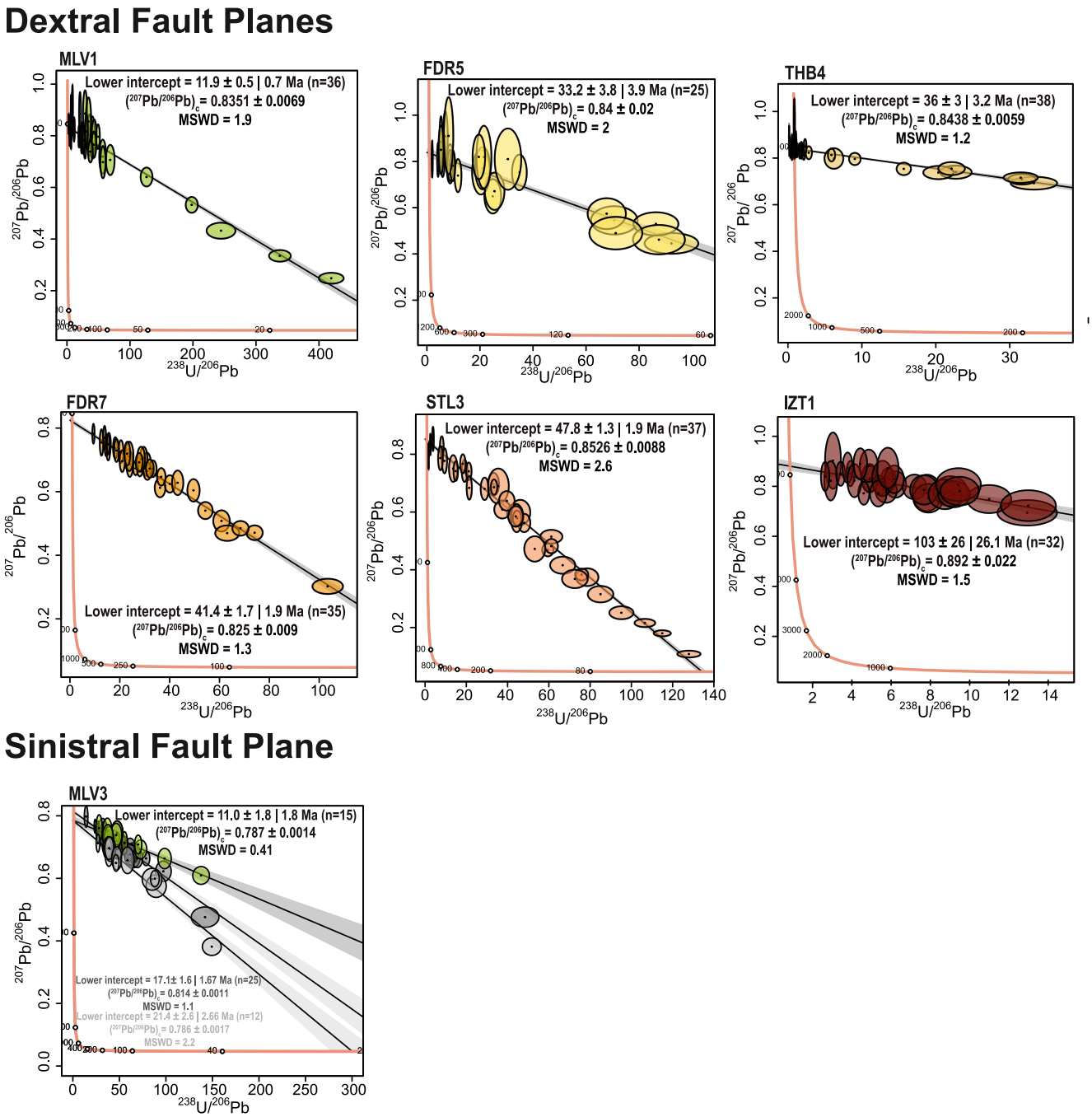


**Figure 5.** (Continued)

rift basins inversion at 84 Ma (Angrand & Mouthereau, 2021; Grool et al., 2018) or 72 Ma (Puigdefàbregas & Souquet, 1986). During this rift inversion phase, deformation is described as equally distributed across the two margins, both by model (Erdős et al., 2015) and tectono-sedimentary studies (Grool et al., 2018). Cruset et al. (2020) date the emplacement of the Upper Pedraforca thrust sheet (Figure 1c) to between 70.6 ± 0.9 Ma and 55.3 ± 0.5 Ma (Figure 7). However, our U-Pb data from syn-kinematic calcite do not show a record of deformation during this first compressive phase of early inversion, from late Maastrichtian to the end of Paleocene (Figure 7). The absence of a deformation record could be attributed to several factors besides tectonic quiescence



19449194, 2025, 2, Downloaded from https://agupubs.onlinelibrary.wiley.com/doi/10.1029/2024TC008634 by Portail BibCNRS INSU, Wiley Online Library on [03/03/2025]. See the Terms and Conditions (https://onlinelibrary.wiley.com/terms-and-conditions) on Wiley Online Library for rules of use; OA articles are governed by the applicable Creative Commons License

**Table 1**
*Brief Sample Description and Associated Calcite U-Pb Geochronology Data*

| Sample | Fault plane | Slickenside | Stratigraphy | Coordinates | U-Pb central age (Ma) | 2σ uncertainty (Ma) | Plane kinematics |
|---|---|---|---|---|---|---|---|
| MLV 3 | N°20–78°W | p41°N | Mid and Lower Aptian | 43,010215°N 0,683407°E | 21,4 | 2,6 | Sinistral |
| | | | | | 17,1 | 1,7 | |
| | | | | | 11 | 1,8 | |
| FDR 5 | N°109–62°S | p114° | Valanginian-Barremian | 43,048250°N 0,729082°E | 33,2 | 3,9 | Dextral |
| FDR 7 | N° 105–64°W | p17°N | Valanginian-Barremian | 43,048250°N 0,729082°E | 41,4 | 1,9 | Dextral |
| IZT 1 | N°114–89°N | p64°E | Mid Aptian Lower Albian | 43,014675°N 0,610880°E | 103 | 26,1 | Dextral |
| THB 4 | N°96–89°N | p27°E | Upper Oxfordian | 42,969973°N 0,591787°E | 36 | 3,2 | Dextral |
| MLV 1 | N° 160–68°W | p21°N | Mid and Lower Aptian | 43,010215°N 0,683407°E | 11,9 | 0,7 | Dextral |
| STL 3 | N°26–52°W | p23°S | Aptian | 42,999375°N 1,134218°E | 47,8 | 1,8 | Dextral |
| LMA 3 | N°109–62°N | p60°E | Lower Thanetian | 43,092189°N 1,381005°E | 37,8 | 1,9 | Flexural slip |
| LMA 4 | N°96–81°N | p84°E | Lower Thanetian | 43,092189°N 1,381005°E | 36,8 | 2,4 | Flexural slip |
| FDR 6 | N°80–39°N | p55°E | Valanginian-Barremian | 43,048250°N 0,729082°E | 30,9 | 5,9 | Flexural slip |
| LT 2 | N°107–79°N | p86°E | Upper Maastrichtian Lower Danian | 42,954083°N 1,863744°E | 30,8 | 2,4 | Flexural slip |
| IZT 6 | N°113–66°N | p73°E | Mid Aptian Lower Albian | 43,014675°N 0,610880°E | 16,3 | 3,2 | Flexural slip |
| CRC 1 | N°099–69°S | p81°W | Lower Thanetian | 42,562621°N 1,795278°E | 43,5 | 1,5 | Flexural slip |
| LT 1 | N°125–67°N | p71°E | Upper Maastrichtian Lower Danian | 42,954083°N 1,863744°E | 47,5 | 8,9 | Flexural slip |
| FDR 1 | N°59–65°N | p86°E | Valanginian-Barremian | 43,048250°N 0,729082°E | 40,8 | 2,2 | Reverse |
| FDR 3 | N°122–27°N | p23°E | Valanginian-Barremian | 43,048250°N 0,729082°E | 34,4 | 1,7 | Reverse |
| RP 2 | N°104–50°N | p83°E | Upper Maastrichtian Dano-Selandian | 42,961343°N 1,775045°E | 48 | 2,4 | Reverse |
| LT 3 | N°100–30°N | p68°E | Upper Maastrichtian Lower Danian | 42,954083°N 1,863744°E | 31,9 | 2,1 | Reverse |
| STL 1 | N°68–46°N | P84°SW | Aptian | 42,999375°N 1,134218°E | 36 | 1,6 | Reverse |
| STL 2 | N°68–46°N | p39°E | Aptian | 42,999375°N 1,134218°E | 42,6 | 5,4 | Reverse |
| STL 4 | N°37–55°W | p59°N | Aptian | 42,999375°N 1,134218°E | 48,5 | 3,1 | Reverse |

*Note.* In addition to the U-Pb central age, given details on the slickenfiber orientation over the fault plane, its kinematics and the age of the formation carrying the microstructure.



19449194, 2025, 2, Downloaded from https://agupubs.onlinelibrary.wiley.com/doi/10.1029/2024TC008634 by Portail BibCNRS INSU, Wiley Online Library on [03/03/2025]. See the Terms and Conditions (https://onlinelibrary.wiley.com/terms-and-conditions) on Wiley Online Library for rules of use; OA articles are governed by the applicable Creative Commons License

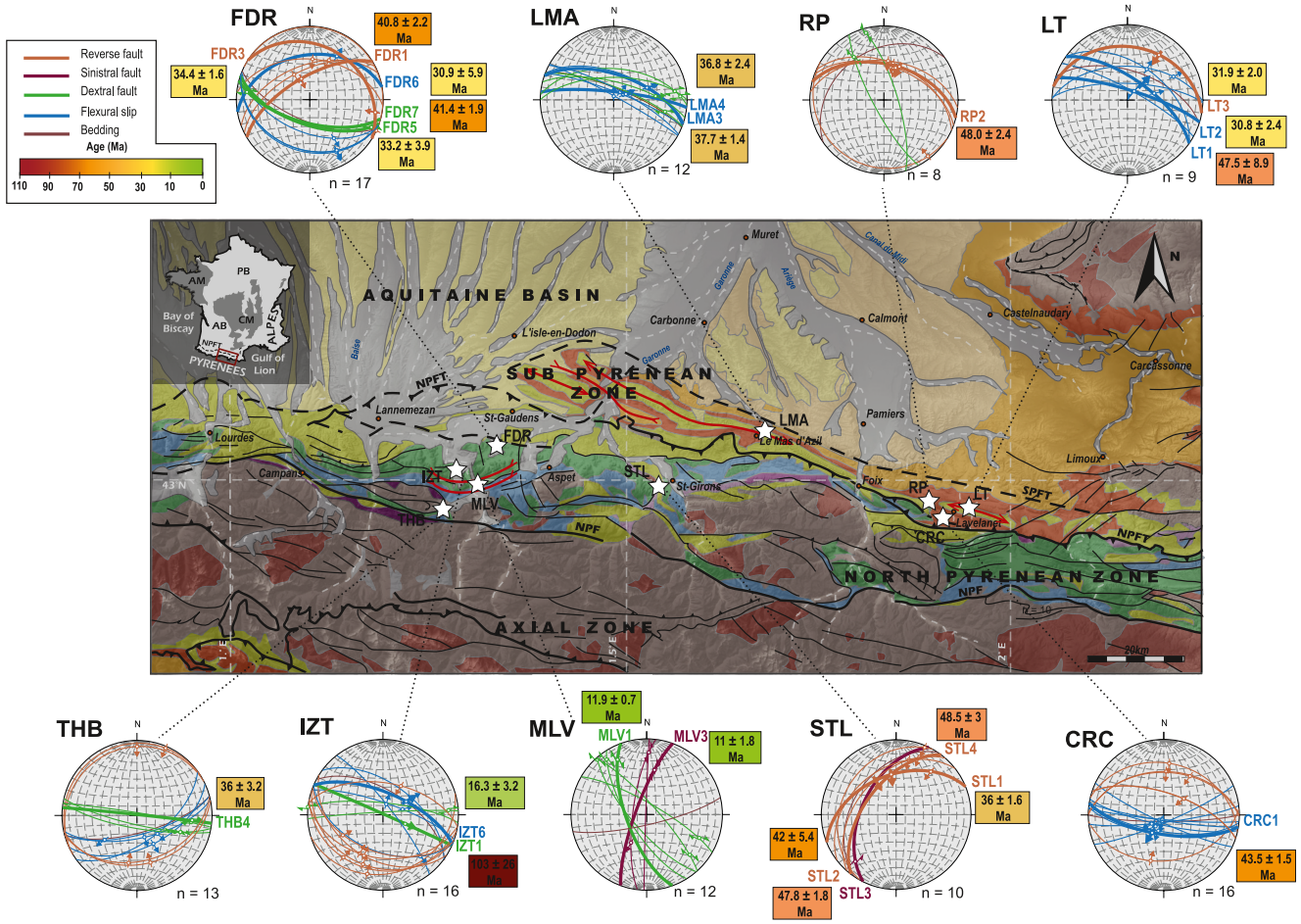


**Figure 6.** Results of U-Pb geochronology and microtectonic study on syn-kinematic calcite slickenfibers. Each dated fault plane is represented on the Wulf lower hemisphere diagram of the sampled site. Sampling site are represented by white stars on a structural map modified after the 1/1 000 000 and 1/50 000 BRGM geological maps of France. U-Pb dates of each plane is given with their 2$\sigma$ error, dated planes are represented in thicker lines on the Wulf diagrams.

in the retro-foreland. The sampled syn-kinematic calcite, possibly of Upper Cretaceous age, may not be suitable for U-Pb carbonate dating due to high Pb or low U concentrations. Factors responsible for such variability in concentration are still poorly understood. Additionally, it is possible that this deformation episode is not associated with the crystallization of slickenfibers.

On a regional scale, the observed absence of tectonic activity in the retro-foreland is consistent with the slow convergence rate between the Eurasian and Iberian plates (Macchiavelli et al., 2017; Mouthereau et al., 2021) during Paleocene. It is the "Paleocene still phase" described by Schettino and Turco (2011). However, this period of quiescence is not as pronounced in the pro-foreland, as shown in Figure 7, and a slow subsidence rate indicates a continuous slow shortening during Paleocene (Grool et al., 2018). These observations do not align with numerical models of inverted rifted margins, which depict roughly symmetrical structures and deformation rates during closure of the exhumed mantle domain and until the onset of subduction of the continental mantle lithosphere (Erdős et al., 2014). Grool et al. (2018) suggests that this asymmetry in the timing of deformation pins down the transition from rift inversion to main collision in a local scale. The creation of a lithospheric fault accommodates deformation during collision (Dielforder et al., 2019), while slow, continuous shortening is recorded in the pro-foreland basin (Cruset et al., 2020; Grool et al., 2018). Continental subduction then leads to a pro-foreland dominant shortening during the main convergence phase (Ford et al., 2022).



19449194, 2025, 2, Downloaded from https://agupubs.onlinelibrary.wiley.com/doi/10.1029/2024TC008634 by Portail BibCNRS INSU, Wiley Online Library on [03/03/2025]. See the Terms and Conditions (https://onlinelibrary.wiley.com/terms-and-conditions) on Wiley Online Library for rules of use; OA articles are governed by the applicable Creative Commons License

10.1029/2024TC008634

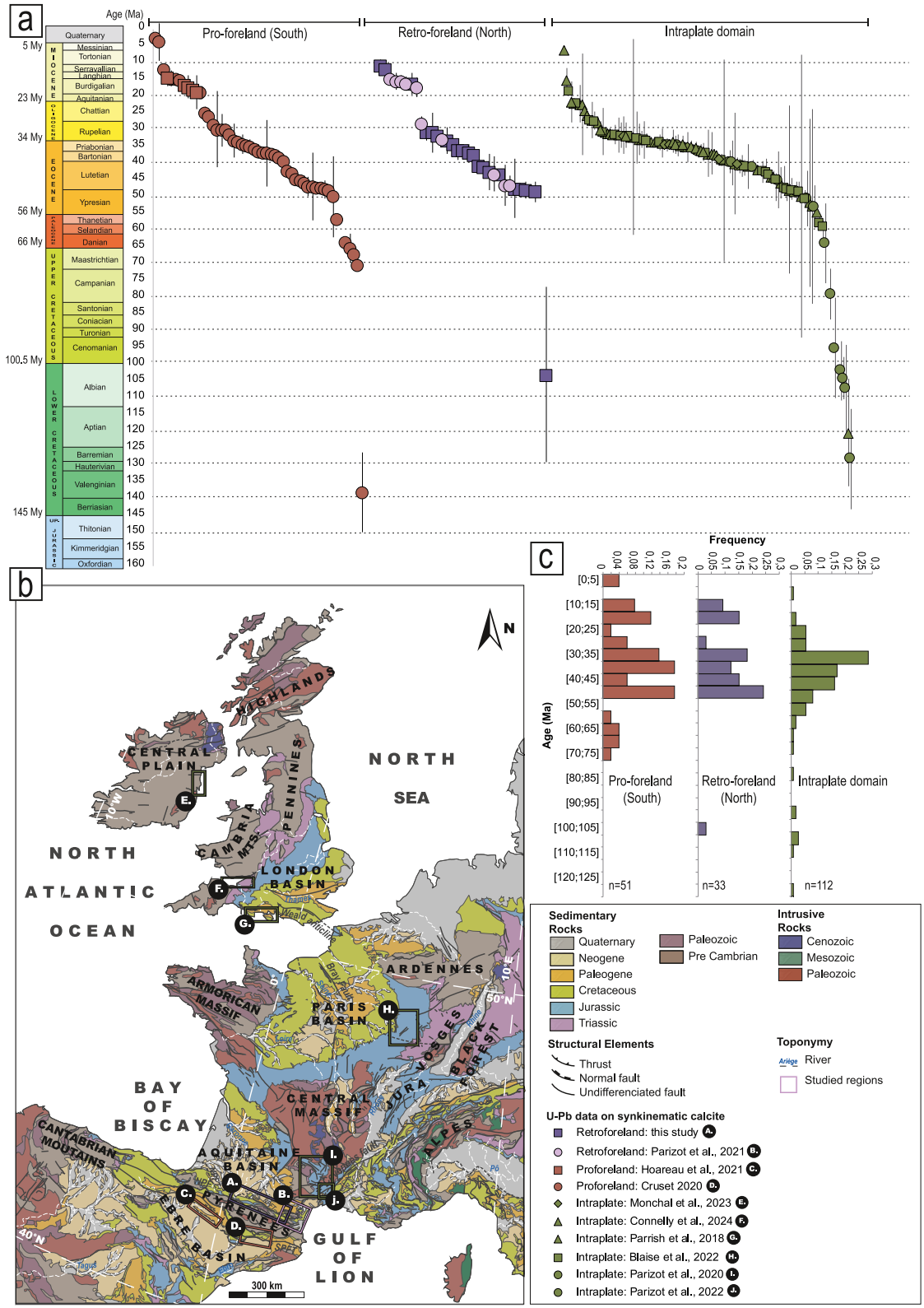


**Figure 7.**



19449194, 2025, 2, Downloaded from https://agupubs.onlinelibrary.wiley.com/doi/10.1029/2024TC008634 by Portail BibCNRS INSU, Wiley Online Library on [03/03/2025]. See the Terms and Conditions (https://onlinelibrary.wiley.com/terms-and-conditions) on Wiley Online Library for rules of use; OA articles are governed by the applicable Creative Commons License

19449194, 2025, 2, Downloaded from https://agupubs.onlinelibrary.wiley.com/doi/10.1029/2024TC008634 by Portail BibCNRS INSU, Wiley Online Library on [03/03/2025]. See the Terms and Conditions (https://onlinelibrary.wiley.com/terms-and-conditions) on Wiley Online Library for rules of use; OA articles are governed by the applicable Creative Commons License

#### 5.2.2. Evolution of Pyrenean Deformation: From Collision to Extension

On both sides of the orogen, main collision starts ca. 48 Ma, 47.7 ± 0.8 Ma in the South Pyrenean Zone (Cruset et al., 2020) (Figures 7 and 8), and 48.5 ± 3 Ma in the North and Sub Pyrenean Zone (this study) (Figures 7 and 8). Thus, although deformation is mainly accommodated in the pro-foreland by the in-sequence emplacement of thin-skin thrust sheets, and thick-skin stacking in the internal zone (Cruset et al., 2020; Erdős et al., 2014; Ford et al., 2016; Grool et al., 2018), in the retro-foreland, deformation is accommodated by a narrower fold-and-thrust belt (Erdős et al., 2014; Grool et al., 2018). While the doubly vergent orogen develops an asymmetrical structure, the formation of brittle structures in both the pro-foreland and the retro-foreland remains synchronous (Figures 7a and 7c). Indeed, fold growth seems to end during Rupelian times, at 29.3 ± 1.8 Ma in the southern part of the Pyrenees (Cruset et al., 2020) and 30.8 ± 2.4 Ma in the northern part (this study) (Figure 7). Furthermore, deformation exhibits remarkable continuity from Ypresian to Rupelian. A quiescent period affects both the pro-foreland and retro-foreland from Chattian to Burdigalian times. Between 30.8 ± 2.4 Ma (LT2) and 16.3 ± 3.2 Ma (IZT6) (Figure 7), our data set shows no evidence of brittle deformation. In the pro-foreland basin, similarly, neither Cruset et al. (2020) nor Hoareau et al. (2021) evidence deformation between middle Chattian and middle Burdigalian. This timeframe coincides with the end of convergence between the European and Iberian plates, which ended during the Aquitanian period (ca. 23–20 Ma), as evidenced by plate reconstructions (Ford et al., 2022; Macchiavelli et al., 2017). However, significant changes in subduction dynamics occurred in the Mediterranean region. The opening of the Gulf of Lion propagated southward in a typical NE-SW direction and first manifested onshore in the Languedoc area where Séranne et al. (2021) recently identified the transition between contractional and extensional regimes during Burdigalian times. Then the eastern Pyrenees underwent dismantling under this extensional regime from late Oligocene to Burdigalian. Our observations align with these previous results. The southern part of the Pyrenees remains under a compressive regime (Cruset et al., 2020), whereas the northeastern part was no longer experiencing compression (this study, Parizot et al., 2021). Meanwhile, the easternmost part was already under an extensional regime (Milesi et al., 2022), associated with the opening of the Gulf of Lion and the southward migration of the subduction system (Jolivet et al., 2021; Milesi et al., 2022; Séranne et al., 2021). The studied area is located north of the Têt fault, which significantly accommodates extension in the easternmost part of the Pyrenees (Jolivet et al., 2021; Taillefer et al., 2021). However, no extensive small-scale brittle structure has been encountered and dated in this area. Hence, extensive deformation might be constrained along major structures. The rifting of the Gulf of Lion ended ca. 23 Ma with the onset of oceanic accretion and the formation of the Algero-Provençal basin (Figure 8d) (Guennoc et al., 2000). From that point onward, extension was accommodated by oceanic accretion, until ca. 16.5–15 Ma (Aslanian et al., 2012; Etheve et al., 2016).

#### 5.2.3. Other Evidence for Miocene Deformation Across the Pyrenean Belt

The Miocene deformation episode is not documented by sedimentation as the top of the continental deposits is poorly dated (Grool et al., 2018), nor by plate reconstructions that set the end of compression in the Pyrenees at the end of Oligocene (Ford et al., 2022; Macchiavelli et al., 2017). However, as thoroughly described in Parizot et al. (2021), during Miocene, the Pyrenees undergo vertical movements resulting in incisions, in the eastern Axial zone, dated by Sartégou et al. (2018) to early Miocene, in the north-western Pyrenees, estimated post Oligocene by Uzel et al. (2019) or even further from the orogen, in the Cévennes area, during Miocene (Serravalian-Tortonian) according to Séranne et al. (2021). Uplift is also recognized during Miocene, by the denudation of massifs in the western Axial Zone (Fillon et al., 2021; Jolivet et al., 2007) and the presence of high elevation denudation surfaces in the Axial Zone (Bosch, Teixell, et al., 2016; Bosch, Van Den Driessche, et al., 2016). While vertical movements are not necessarily accompanied by horizontal displacements (Teixell et al., 2009), U-Pb geochronology on syn-kinematic calcite provides evidence for horizontal Miocene deformation in both the pro-foreland

**Figure 7.** Compilation of existing U-Pb age-constraints on brittle deformation on Pyrenean forelands and the West European platform intraplate domain. Ages are represented by colored dots with their uncertainties ($2\sigma$). (a) Red dots represent U-Pb ages on the pro-foreland basin (South Pyrenean Zone) (Cruset et al., 2020; Hoareau et al., 2021). Purple dots represent ages on the retro-foreland basin (Purple: this study, pink: Parizot et al., 2021). Green dots represent ages on the intraplate domain (Blaise et al., 2022; Connolly et al., 2024; Monchal et al., 2023; Parizot et al., 2020, 2022; Parrish et al., 2018). (b) Structural map of Europe modified after the European Geological Data Infrastructure (EGDI) 1/1 000 000 geological map. Boxes represent the different study area used in this compilation. (c) Normalized histograms of U-Pb calcite ages on the Pyrenean pro-foreland basin, retro-foreland basin and on the intraplate domain. Histogram binning = 5 Ma, data are plotted without considering the corresponding age uncertainties.

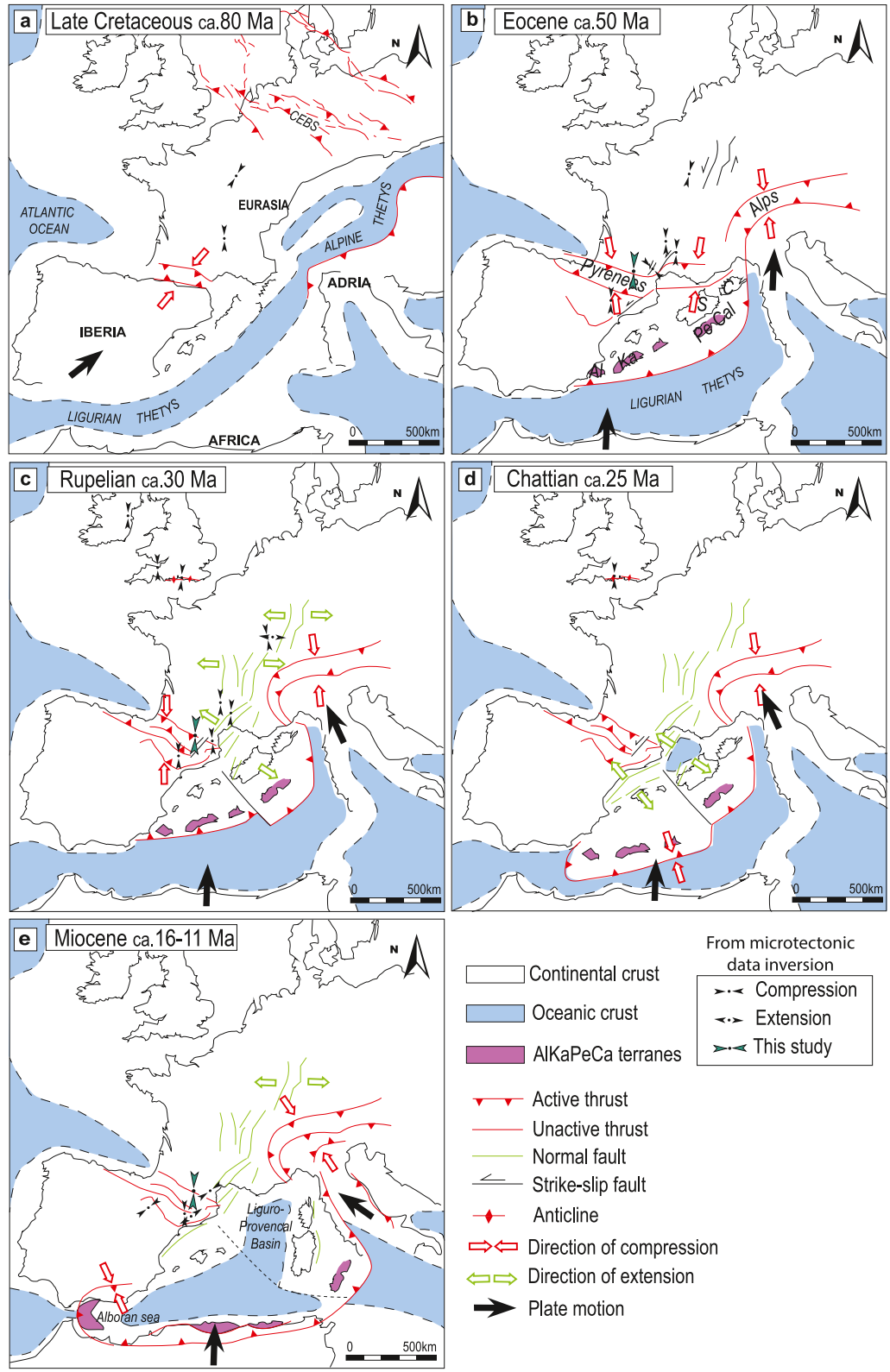


**Figure 8.** Schematic representation of the evolution of the Western Mediterranean and western Europe geodynamics, from late Mesozoic to Miocene, modified after Dèzes et al. (2004), Dielforder et al. (2019), Etheve et al. (2016), Jolivet (2023), and Séranne (1999). Structural data (Blaise et al., 2022; Connolly et al., 2024; Cruset et al., 2020; Hoareau et al., 2021; Monchal et al., 2023; Parizot et al., 2021, 2022; Parrish et al., 2018). See text for discussion.



19449194, 2025, 2, Downloaded from https://agupubs.onlinelibrary.wiley.com/doi/10.1029/2024TC008634 by Portail BibCNRS INSU, Wiley Online Library on [03/03/2025]. See the Terms and Conditions (https://onlinelibrary.wiley.com/terms-and-conditions) on Wiley Online Library for rules of use; OA articles are governed by the applicable Creative Commons License

19449194, 2025, 2, Downloaded from https://agupubs.onlinelibrary.wiley.com/doi/10.1029/2024TC008634 by Portail BibCNRS INSU, Wiley Online Library on [03/03/2025]. See the Terms and Conditions (https://onlinelibrary.wiley.com/terms-and-conditions) on Wiley Online Library for rules of use; OA articles are governed by the applicable Creative Commons License

(Cruset et al., 2020; Hoareau et al., 2021) and retro-foreland basins (this study, Parizot et al., 2021). Whether these data indicate exhumation (Cruset et al., 2020) or brittle compressive deformation (Hoareau et al., 2021; Parizot et al., 2021), they reveal a regional Miocene deformation episode that lasted from late Burdigalian to Tortonian, occurring synchronously in both the pro-foreland and retro-foreland basin. The origin of these movements remains unclear. Ortiz et al. (2020) proposes that the whole West European domain would be uplifted by a mantle-controlled mechanism. Both Fillon et al. (2021) and Cruset et al. (2020) associate this Miocene deformation episode with normal faulting and the dismantling of the belt. However, Fillon et al. (2021) correlates the high erosion in the northwestern Pyrenees with WNW-ESE Quaternary faults at the boundary with the Axial Zone, while Cruset et al. (2020) date, in the Pedraforca thrust sheets, Miocene normal faults indicating a NE-SW extension synchronous with E-W trending reverse faults. On the other hand, Parizot et al. (2021) in the Corbières area and Hoareau et al. (2021) in the Jaca basin both propose that the Pyrenees were under a compressive regime during Burdigalian-Langhian. This study reveals an episode of horizontal deformation during Miocene, characterized by reactivation of flexural slip planes (IZT6) and the formation of conjugated strike-slip fault planes (MLV1 and MLV3) (Figure 2). These sampled planes are associated with large-scale compressive structures (Figure 1).

### 5.3. Timeline of Stress Propagation Toward the Intraplate Domain

Boundary forces induce horizontal stress far away across tectonic plates as the result of stress propagation. Intraplate deformation is described as occurring during major changes of the geodynamic setting at plate boundaries, and more specifically, in a converging setting (Bosworth et al., 1999; Sutherland et al., 2017), at the onset of convergence and during the formation of a plate boundary fault (Dielforder et al., 2019). In previous section, the timing of deformation in the asymmetrical Pyrenean orogen has been discussed. By examining here how the intraplate domain responds, the aim is to refine the spatio-temporal evolution of deformation and whether intraplate responds simultaneously to deformation at boundary.

The aperture of the Pyrenean basins in the early Cretaceous is not documented by calcite U-Pb geochronology data in the orogen. Yet, in the Grands Causses area, Parizot et al. (2020) showed that some normal faults, prior associated with the Alpine Tethys Ocean opening were in fact early Cretaceous in age and more probably linked to the opening of the Pyrenean basins, however data are scarce and carry high uncertainties (Figure 7a).

In the Central European Basin System (CEBS), Triassic to early Cretaceous NW-trending basins are inverted, and major faults are reactivated in dip-slip contraction by a uniform N to NE-trending compressive stress (Kley & Voigt, 2008; Navabpour et al., 2017; Nielsen et al., 2005; Scheck-Wenderoth & Lamarche, 2005) (Figure 8a). This main shortening event is dated between latest Turonian and Campanian (ca. 90 to 72 Ma) (Ziegler et al., 1995). Although traditionally attributed to early Alpine orogeny, Kley and Voigt (2008) demonstrate that it coincides with the onset of Africa-Iberia-Europe convergence. Yet, this early Pyrenean phase of convergence (Grool et al., 2018) is barely represented, as U-Pb geochronology data are scarce, and only a few small-scale brittle structures seem to record this deformation phase in the Pyrenean orogen within the intraplate domain (Cruset et al., 2020; Parizot et al., 2020) (Figures 7 and 8a).

The Paleocene (ca. 66 to 56 Ma) is characterized by a phase of tectonic quiescence, with little to no deformation recorded during this time. This period of stability can be attributed to the transition from basin inversion to continental subduction in the Pyrenees, as well as a decrease in the convergence rate between Africa, Iberia, and Europe (Dielforder et al., 2019). However, mechanical considerations, numerical simulations, and geological reconstructions all suggest that the plate boundary fault between Europe and Iberia weakened the mechanical coupling between the plates, reducing the strength of the lithosphere and its ability to transmit compressive stress, suggesting that intraplate deformation did not resume after the Paleocene (Dielforder et al., 2019; Ford et al., 2022).

Yet, several studies, on U-Pb geochronology of syn-kinematic calcite, have highlighted tectonic activity under N-S compressive stress in the intraplate domain as the Pyrenean orogenic prism was building up (Blaise et al., 2022; Connolly et al., 2024; Monchal et al., 2023; Parizot et al., 2020, 2022; Parrish et al., 2018) (Figures 8b and 8c). Ages presented on Figure 7 in the intraplate domain date a great variety of structures, from reactivated faults (Parizot et al., 2020) and folds (Monchal et al., 2023), neoformed folds and faults (Connolly et al., 2024; Parizot et al., 2021; Parrish et al., 2018) or even syn-tectonic veins and tension gashes networks (Blaise et al., 2022). Ages mainly span from ca. 55 to 30 Ma, all structures are consistent with a N-S contraction and interpreted as the

19449194, 2025, 2, Downloaded from https://agupubs.onlinelibrary.wiley.com/doi/10.1029/2024TC008634 by Portail BibCNRS INSU, Wiley Online Library on [03/03/2025]. See the Terms and Conditions (https://onlinelibrary.wiley.com/terms-and-conditions) on Wiley Online Library for rules of use; OA articles are governed by the applicable Creative Commons License

expression of far-field stress from the Pyrenean orogen (Figures 8b and 8c). The compressive episode at ca. 48 Ma evidenced in the northern Pyrenees (this study), and east of the Paris Basin (Blaise et al., 2022), is coherent with the emersion of the Paris Basin (Briais et al., 2016) or the uplift of the Brabant, north of the Ardennes (Figure 7) (Vandenberghe et al., 2004). This N-S compressive episode affects all Western Europe and appears to mark the onset of continental convergence between Iberia and Europe. Although some of the tension gashes dated in the eastern Paris Basin between ca. 40 and 35 Ma (Blaise et al., 2022) (Figures 7a and 7c) could either be linked to the opening of the European Central Rift System (ECRIS) (Ring & Gerdes, 2016) or the Pyrenean orogen, the complete data set compiled here shows strikingly well how intraplate domain deformed synchronously to Pyrenean domain and major geodynamic events at plate borders.

In the east of the Paris Basin post-Rupelian (ca. 28 Ma) brittle structures are scarce (Blaise et al., 2022), with no tension gashes recorded between approximately ca. 27 and 22 Ma, indicating a period of tectonic quiescence (Figure 8d), even though Parrish et al. (2018) dates minor deformed fractures at ca. 25 Ma and younger in a few localities. The most recent ages obtained by Parrish et al. (2018) are based on void-filling samples, and their structural origin has yet to be proven, even though they indicate a recent episode of fluid circulation in the Hampshire Basin.

As discussed in Section 5.2, the Pyrenean orogen underwent a phase of deformation during Miocene. Some authors highlight vertical movements (Fillon et al., 2021; Ortiz et al., 2020; Sartégou et al., 2018) and studies on U-Pb dating of fault calcite have demonstrated the existence of horizontal movements (this study; Hoareau et al., 2021; Parizot et al., 2021), likely associated with contractional deformation. Data from both sides of the Pyrenean range shows that between Burdigalian and Serravalian, the entire Pyrenees might have been under a compressive stress regime. The geodynamic process responsible for this deformation event has not yet been well identified. As suggested by several authors (Etheve et al., 2016; Frizon De Lamotte et al., 2000; Parizot et al., 2021), starting from ca.17 Ma (Abbassene et al., 2016) the Kabylies, from the Alboran, Kabylian, Peloritan and Calabrian (AlKaPeCa) terranes (Bouillin et al., 1986), are accreted along the North African margin where the Ligurian-Tethys is fully subducted (Figure 8e). This major change in the west Mediterranean geodynamic settings would restore a strong coupling along a N/S Eurasia/Iberia/Africa transect (Frizon De Lamotte et al., 2000; Parizot et al., 2021). We propose that this late event could be the far-field expression of the collision between the Kabylies and the North African margin and the building of the Tell belt.

As previously discussed, Dielforder et al. (2019) and Ford et al. (2022) suggest that deformation in the intraplate domain ceased after the Paleocene quiescence due to the formation of a rheologically weak plate boundary fault between Iberia and Europe. The dating of tectonic calcite from the intraplate domain shows that it is probably more deformed than previously assumed over the Paleogene-Neogene period. Although the brittle deformation recorded since the Eocene in the intraplate domain is less intense compared to the inversion of Central Europe Basins (Dielforder et al., 2019; Kley & Voigt, 2008), it still exhibits a stress field that is strongly correlated to the activity at African-Iberian-European plate boundaries, in a notably synchronous manner.

## 6. Conclusions

This study highlights the protracted history of brittle deformation in the Pyrenean orogen, its forelands and its intraplate domain, from upper Cretaceous to Miocene times, within the context of western Mediterranean geodynamics, controlled by the convergence of Africa, Iberia and Eurasia. It presents new absolute time constraints on the northern part of the Pyrenean orogen and integrates these results with other published U-Pb geochronology data.

1. In the northern part of the Pyrenees, deformation and folding events are continuous from ca. 48 Ma to 30 Ma during the convergence of Iberia and Europe. This is followed by a period of tectonic quiescence from ca. 30 Ma to 16 Ma, coinciding broadly with the rifting of the Gulf of Lion and then the oceanic accretion within the Liguro-Provençal basin. Eventually, the retro-foreland basin records an episode of horizontal Miocene deformation consistent with a N-S trending $\sigma 1$.
2. While shortening during Eocene time is mainly absorbed by the pro-foreland basin, both forelands of the Pyrenean orogen experience synchronous deformation.
3. Deformation in the intraplate domain also occurred under N-S compressive stress from the Eocene to the late Oligocene, showing synchronous tectonic activity with the Pyrenean orogen.

Therefore, an extensive data set of U-Pb dating of syntectonic structures sheds a new light on the way foreland basins reacts to plate boundary convergent events, and the way stresses are transmitted or not far away in the intraplate domain.

## Conflict of Interest

The authors declare no conflicts of interest relevant to this study.

## Data Availability Statement

The data that support the findings of this study are available in Supporting Information S1 of this article. All new data presented on this article are available to the public at the data sharing infrastructure of Mendeley Data (Jullien-Sicre et al., 2025) in the following data repository: https://doi.org/10.17632/8mr86grhnk.1.

**Acknowledgments**
This work is part of A. Jullien-Sicre, PhD funded by a Paris-Saclay University research grant (ED SMEMAG). It was also supported by the TelluS Program of CNRS-INSU. We wish to express our gratitude to Sarah Bowie, Catherine Mottram, and Perach Nuriel who provided very useful comments to improve the quality of the manuscript.

## References

Abbassene, F., Chazot, G., Bellon, H., Bruguier, O., Ouabadi, A., Maury, R. C., et al. (2016). A 17 Ma onset for the post-collisional K-rich calc-alkaline magmatism in the Maghrebides: Evidence from Bougaroun (northeastern Algeria) and geodynamic implications. *Tectonophysics*, *674*, 114–134. https://doi.org/10.1016/j.tecto.2016.02.013

Al Reda, S. M., Barbarand, J., Gautheron, C., Lasseur, E., Loget, N., Pinna-Jamme, R., & Briais, J. (2021). Thermal record of the building of an orogen in the retro-foreland basin: Insight from basement and detrital thermochronology in the eastern Pyrenees and the north Pyrenean basin (France). *Basin Research*, *33*(5), 2763–2791. https://doi.org/10.1111/bre.12583

Andrieu, S., Saspiturry, N., Lartigau, M., Issautier, B., Angrand, P., & Lasseur, E. (2021). Large-scale vertical movements in Cenomanian to Santonian carbonate platform in Iberia: Indicators of a Coniacian pre-orogenic compressive stress. *BSGF - Earth Sciences Bulletin*, *192*(1), 19. https://doi.org/10.1051/bsgf/2021011

Angelier, J., & Mechler, P. (1977). Sur une methode graphique de recherche des contraintes principales egalement utilisables en tectonique et en seismologie: La methode des diedres droits. *Bulletin de la Societe Geologique de France*, *7*(6), 1309–1318. https://doi.org/10.2113/gssgfbull.S7-XIX.6.1309

Angrand, P., Ford, M., & Watts, A. B. (2018). Lateral variations in Foreland flexure of a rifted continental margin: The Aquitaine Basin (SW France). *Tectonics*, *37*(2), 430–449. https://doi.org/10.1002/2017TC004670

Angrand, P., & Mouthereau, F. (2021). Evolution of the Alpine orogenic belts in the Western Mediterranean region as resolved by the kinematics of the Europe-Africa diffuse plate boundary. *BSGF - Earth Sciences Bulletin*, *192*, 42. https://doi.org/10.1051/bsgf/2021031

Arenas, C., Millán, H., Pardo, G., & Pocoví, A. (2001). Ebro Basin continental sedimentation associated with late compressional Pyrenean tectonics (north-eastern Iberia): Controls on basin margin fans and fluvial systems. *Basin Research*, *13*(1), 65–89. https://doi.org/10.1046/j.1365-2117.2001.00141.x

Aslanian, D., Moulin, M., Schnurle, P., Klingelhoefer, F., Leroux, E., Rabineau, M., et al. (2012). Structure and evolution of the Gulf of Lions: The Sardinia seismic experiment and the GOLD (Gulf of Lions Drilling) project. *The Leading Edge*, *31*(7), 786–792. https://doi.org/10.1190/tle31070786.1

Baby, P., Crouzet, G., Specht, M., Deramond, J., Bilotte, M., & Debroas, E.-J. (1988). Rôle des paléostructures albo-cénomaniennes dans la géométrie des chevauchements frontaux nord-pyrénéens. *Académies Des Sciences de Paris*, *306*(4), 307–313.

Barbarand, J., Quesnel, F., & Pagel, M. (2013). Lower Paleogene denudation of Upper Cretaceous cover of the Morvan Massif and southeastern Paris Basin (France) revealed by AFT thermochronology and constrained by stratigraphy and paleosurfaces. *Tectonophysics*, *608*, 1310–1327. https://doi.org/10.1016/j.tecto.2013.06.011

Benedicto, A., Labaume, P., Séguret, M., & Séranne, M. (1996). Low-angle crustal ramp and basin geometry in the Gulf of Lion passive margin: Oligocene-Aquitanian Vistrenque graben, SE France. *Tectonics*, *15*(6), 1192–1212. https://doi.org/10.1029/96TC01097

Bergerat, F. (1987). Stress fields in the European platform at the time of Africa-Eurasia collision. *Tectonics*, *6*(2), 99–132. https://doi.org/10.1029/TC006i002p00099

Bestani, L., Espurt, N., Lamarche, J., Floquet, M., Philip, J., Bellier, O., & Hollender, F. (2015). Structural style and evolution of the Pyrenean-Provence thrust belt, SE France. *Bulletin de la Societe Geologique de France*, *186*(4–5), 223–241. https://doi.org/10.2113/gssgfbull.186.4-5.223

Bilotte, M. (1978). Evolution sedimentaire et tectonique du bassin sous-pyreneen a la fin du Cretace a l'Est de la Garonne. *Bulletin de la Societe Geologique de France*, *7*(5), 649–655. https://doi.org/10.2113/gssgfbull.s7-xx.5.649

Bilotte, M., Cosson, J., Crochet, B., Peybernès, B., Roche, J., Taillefer, F., & Villatte, J. (1988). Notice explicative de la feuille Lavelanet à 1/50 000 (Feuille No. 1076).

Blaise, T., Ali Khoudja, S. A., Carpentier, C., Brigaud, B., Missenard, Y., Mangenot, X., et al. (2022). Far-field brittle deformation record in the eastern Paris Basin (France). *Geological Magazine*, *159*(11–12), 1–15. https://doi.org/10.1017/S0016756822000772

Bons, P. D., Elburg, M. A., & Gomez-Rivas, E. (2012). A review of the formation of tectonic veins and their microstructures. *Journal of Structural Geology*, *43*, 33–62. https://doi.org/10.1016/j.jsg.2012.07.005

Bosch, G. V., Teixell, A., Jolivet, M., Labaume, P., Stockli, D., Domènech, M., & Monié, P. (2016). Timing of Eocene–Miocene thrust activity in the Western Axial Zone and Chaînons Béarnais (west-central Pyrenees) revealed by multi-method thermochronology. *Comptes Rendus Geoscience*, *348*(3–4), 246–256. https://doi.org/10.1016/j.crte.2016.01.001

Bosch, G. V., Van Den Driessche, J., Babault, J., Robert, A., Carballo, A., Le Carlier, C., et al. (2016). Peneplanation and lithosphere dynamics in the Pyrenees. *Comptes Rendus Geoscience*, *348*(3–4), 194–202. https://doi.org/10.1016/j.crte.2015.08.005

Bosworth, W., Guiraud, R., & Kessler, L. G. (1999). Late Cretaceous (ca. 84 Ma) compressive deformation of the stable platform of northeast Africa (Egypt): Far-field stress effects of the "Santonian event" and origin of the Syrian arc deformation belt. *Geology*, *27*(7), 633. https://doi.org/10.1130/0091-7613(1999)027<0633:LCCMCD>2.3.CO;2

Bouillin, J.-P., Durand-Delga, M., & Olivier, P. (1986). Betic-Rifian and Tyrrhenian Arcs: Distinctive Features. *Genesis and Development Stages*, *21*, 281–304. https://doi.org/10.1016/B978-0-444-42688-8.50017-5



19449194, 2025, 2, Downloaded from https://agupubs.onlinelibrary.wiley.com/doi/10.1029/2024TC008634 by Portail BibCNRS INSU, Wiley Online Library on [03/03/2025]. See the Terms and Conditions (https://onlinelibrary.wiley.com/terms-and-conditions) on Wiley Online Library for rules of use; OA articles are governed by the applicable Creative Commons License

Briais, J., Guillocheau, F., Lasseur, E., Robin, C., Châteauneuf, J.-J., & Serrano, O. (2016). Response of a low-subsiding intracratonic basin to long wavelength deformations: The Palaeocene–early Eocene period in the Paris Basin. *Solid Earth*, *7*(1), 205–228. https://doi.org/10.5194/se-7-205-2016

Canérot, J. (2017). The pull apart-type Tardets-Mauléon Basin, a key to understand the formation of the Pyrenees. *Bulletin de la Societe Geologique de France*, *188*(6), 35. https://doi.org/10.1051/bsgf/2017198

Cavaillé, A., Debat, P., & Calas, G. (1975). Notice explicative de la feuille Castelnaudary à 1/50 000 (Feuille No. 1036).

Choukroune, P. (1976). A Discussion on natural strain and geological structure - Strain patterns in the Pyrenean Chain. *Philosophical Transactions of the Royal Society of London - Series A: Mathematical and Physical Sciences*, *283*(1312), 271–280. https://doi.org/10.1098/rsta.1976.0084

Choukroune, P. (1989). The ECORS Pyrenean deep seismic profile reflection data and the overall structure of an orogenic belt. *Tectonics*, *8*(1), 23–39. https://doi.org/10.1029/TC008i001p00023

Choukroune, P., & Delair, J. (1976). Un modele cinematique de la fracturation liee au plissement concentrique; l'exemple des Petites Pyrenees. *Bulletin de la Societe Geologique de France*, *7*(6), 1591–1597. https://doi.org/10.2113/gssgfbull.S7-XVIII.6.1591

Choukroune, P., & Mattauer, M. (1978). Tectonique des plaques et Pyrénées; sur le fonctionnement de la faille transformante nord-pyrénéenne; comparaisons avec des modèles actuels. *BSGF - Earth Sciences Bulletin*, *20*(5), 689–700. https://doi.org/10.2113/gssgfbull.S7-XX.5.689

Christophoul, F., Soula, J.-C., Brusset, S., Elibana, B., Roddaz, M., Bessiere, G., & Deramond, J. (2003). Time, place and mode of propagation of foreland basin systems as recorded by the sedimentary fill: Examples of the Late Cretaceous and Eocene retro-foreland basins of the north-eastern Pyrenees. *Geological Society, London, Special Publications*, *208*(1), 229–252. https://doi.org/10.1144/GSL.SP.2003.208.01.11

Clerc, C., Lahfid, A., Monié, P., Lagabrielle, Y., Chopin, C., Poujol, M., et al. (2015). High-temperature metamorphism during extreme thinning of the continental crust: A reappraisal of the North Pyrenean passive paleomargin. *Solid Earth*, *6*(2), 643–668. https://doi.org/10.5194/se-6-643-2015

Cloetingh, S., Burov, E., & Poliakov, A. (1999). Lithosphere folding: Primary response to compression? (from central Asia to Paris basin). *Tectonics*, *18*(6), 1064–1083. https://doi.org/10.1029/1999TC900040

Connolly, J., Anderson, M., Mottram, C., Price, G. D., Parrish, R., & Sanderson, D. (2024). Using U–Pb carbonate dating to constrain the timing of extension and fault reactivation within the Bristol Channel Basin, SW England. *Journal of the Geological Society*, *181*(5), jgs2024-021. https://doi.org/10.1144/jgs2024-021

Cruset, D., Vergés, J., Albert, R., Gerdes, A., Benedicto, A., Cantarero, I., & Travé, A. (2020). Quantifying deformation processes in the SE Pyrenees using U–Pb dating of fracture-filling calcites. *Journal of the Geological Society*, *177*(6), 1186–1196. https://doi.org/10.1144/jgs2020-014

Debroas, E. J. (1990). Le flysch noir albo-cenomanien temoin de la structuration albienne a senonienne de la Zone nord-pyreneenne en Bigorre (Hautes-Pyrenees, France). *Bulletin de la Societe Geologique de France*, *6*(2), 273–285. https://doi.org/10.2113/gssgfbull.VI.2.273

Delvaux, D., & Sperner, B. (2003). New aspects of tectonic stress inversion with reference to the TENSOR program. *Geological Society, London, Special Publications*, *212*(1), 75–100. https://doi.org/10.1144/GSL.SP.2003.212.01.06

Dèzes, P., Schmid, S. M., & Ziegler, P. A. (2004). Evolution of the European Cenozoic Rift System: Interaction of the Alpine and Pyrenean orogens with their foreland lithosphere. *Tectonophysics*, *389*(1–2), 1–33. https://doi.org/10.1016/j.tecto.2004.06.011

Dielforder, A., Frasca, G., Brune, S., & Ford, M. (2019). Formation of the Iberian-European convergent plate boundary fault and its effect on intraplate deformation in Central Europe. *Geochemistry, Geophysics, Geosystems*, *20*(5), 2395–2417. https://doi.org/10.1029/2018GC007840

Doblas, M. (1998). Slickenside kinematic indicators. *Tectonophysics*, *295*(1–2), 187–197. https://doi.org/10.1016/S0040-1951(98)00120-6

Ducoux, M., Masini, E., Tugend, J., Gómez-Romeu, J., & Calassou, S. (2022). Basement-decoupled hyperextension rifting: The tectono-stratigraphic record of the salt-rich Pyrenean necking zone (Arzacq Basin, SW France). *GSA Bulletin*, *134*(3–4), 941–964. https://doi.org/10.1130/B35974.1

Erdős, Z., Huismans, R. S., & Van Der Beek, P. (2015). First-order control of syntectonic sedimentation on crustal-scale structure of mountain belts. *Journal of Geophysical Research: Solid Earth*, *120*(7), 5362–5377. https://doi.org/10.1002/2014JB011785

Erdős, Z., Huismans, R. S., Van Der Beek, P., & Thieulot, C. (2014). Extensional inheritance and surface processes as controlling factors of mountain belt structure. *Journal of Geophysical Research: Solid Earth*, *119*(12), 9042–9061. https://doi.org/10.1002/2014JB011408

Ershov, A. V., Brunet, M.-F., Nikishin, A. M., Bolotov, S. N., Nazarevich, B. P., & Korotaev, M. V. (2003). Northern Caucasus basin: Thermal history and synthesis of subsidence models. *Sedimentary Geology*, *156*(1–4), 95–118. https://doi.org/10.1016/S0037-0738(02)00284-1

Etheve, N., Frizon De Lamotte, D., Mohn, G., Martos, R., Roca, E., & Blanpied, C. (2016). Extensional vs contractional Cenozoic deformation in Ibiza (Balearic Promontory, Spain): Integration in the West Mediterranean back-arc setting. *Tectonophysics*, *682*, 35–55. https://doi.org/10.1016/j.tecto.2016.05.037

Fillon, C., Gautheron, C., & van der Beek, P. (2013). Oligocene–Miocene burial and exhumation of the Southern Pyrenean foreland quantified by low-temperature thermochronology. *Journal of the Geological Society*, *170*(1), 67–77. https://doi.org/10.1144/jgs2012-051

Fillon, C., Mouthereau, F., Calassou, S., Pik, R., Bellahsen, N., Gautheron, C., et al. (2021). Post-orogenic exhumation in the western Pyrenees: Evidence for extension driven by pre-orogenic inheritance. *Journal of the Geological Society*, *178*(2), jgs2020-079. https://doi.org/10.1144/jgs2020-079

Ford, M., Hemmer, L., Vacherat, A., Gallagher, K., & Christophoul, F. (2016). Retro-wedge foreland basin evolution along the ECORS line, eastern Pyrenees, France. *Journal of the Geological Society*, *173*(3), 419–437. https://doi.org/10.1144/jgs2015-129

Ford, M., Masini, E., Vergés, J., Pik, R., Ternois, S., Léger, J., et al. (2022). Evolution of a low convergence collisional orogen: A review of Pyrenean orogenesis. *BSGF - Earth Sciences Bulletin*, *193*(1), 19. https://doi.org/10.1051/bsgf/2022018

Frizon De Lamotte, D., Saint Bezar, B., Bracène, R., & Mercier, E. (2000). The two main steps of the Atlas building and geodynamics of the western Mediterranean. *Tectonics*, *19*(4), 740–761. https://doi.org/10.1029/2000TC900003

Gerbault, M., Burov, E. B., Poliakov, A. N. B., & Daignières, M. (1999). Do faults trigger folding in the lithosphere? *Geophysical Research Letters*, *26*(2), 271–274. https://doi.org/10.1029/1998GL900293

Golberg, J. M., & Leyreloup, A. F. (1990). High temperature-low pressure Cretaceous metamorphism related to crustal thinning (Eastern North Pyrenean Zone, France). *Contributions to Mineralogy and Petrology*, *104*(2), 194–207. https://doi.org/10.1007/BF00306443

Grool, A. R., Ford, M., Vergés, J., Huismans, R. S., Christophoul, F., & Dielforder, A. (2018). Insights into the crustal-scale dynamics of a doubly vergent orogen from a quantitative analysis of its forelands: A case study of the Eastern Pyrenees. *Tectonics*, *37*(2), 450–476. https://doi.org/10.1002/2017TC004731

Guennoc, P., Gorini, C., & Mauffret, A. (2000). Histoire géologique du golfe du Lion et cartographie du rift oligo-aquitanien et de la surface messinienne. *Géologie de la France*, *3*, 67–97.

Guillong, M., Samankassou, E., Müller, I. A., Szymanowski, D., Looser, N., Tavazzani, L., et al. (2024). Technical note: RA138 Calcite U-Pb LA-ICP-MS primary reference material. https://doi.org/10.5194/gchron-2024-7



19449194, 2025, 2, Downloaded from https://agupubs.onlinelibrary.wiley.com/doi/10.1029/2024TC008634 by Portail BibCNRS INSU, Wiley Online Library on [03/03/2025]. See the Terms and Conditions (https://onlinelibrary.wiley.com/terms-and-conditions) on Wiley Online Library for rules of use; OA articles are governed by the applicable Creative Commons License

Guillong, M., Wotzlaw, J.-F., Looser, N., & Laurent, O. (2020). *New analytical and data evaluation protocols to improve the reliability of U-Pb LA-ICP-MS carbonate dating* (preprint). SIMS, LA-ICP-MS. https://doi.org/10.5194/gchron-2019-20

Hancock, P. L. (1985). Brittle microtectonics: Principles and practice. *Journal of Structural Geology*, *7*(3–4), 437–457. https://doi.org/10.1016/0191-8141(85)90048-3

Hoareau, G., Crognier, N., Lacroix, B., Aubourg, C., Roberts, N. M. W., Niemi, N., et al. (2021). Combination of Δ47 and U-Pb dating in tectonic calcite veins unravel the last pulses related to the Pyrenean Shortening (Spain). *Earth and Planetary Science Letters*, *553*, 116636. https://doi.org/10.1016/j.epsl.2020.116636

Hoth, S., Kukowski, N., & Oncken, O. (2008). Distant effects in bivergent orogenic belts—How retro-wedge erosion triggers resource formation in pro-foreland basins. *Earth and Planetary Science Letters*, *273*(1–2), 28–37. https://doi.org/10.1016/j.epsl.2008.05.033

Jolivet, L. (2023). Tethys and Apulia (Adria), 100 years of reconstructions. *Comptes Rendus Geoscience*, *355*(S2), 1–20. https://doi.org/10.5802/crgeos.198

Jolivet, L., Baudin, T., Calassou, S., Chevrot, S., Ford, M., Issautier, B., et al. (2021). Geodynamic evolution of a wide plate boundary in the Western Mediterranean, near-field *versus* far-field interactions. *BSGF - Earth Sciences Bulletin*, *192*, 48. https://doi.org/10.1051/bsgf/2021043

Jolivet, L., & Faccenna, C. (2000). Mediterranean extension and the Africa-Eurasia collision. *Tectonics*, *19*(6), 1095–1106. https://doi.org/10.1029/2000TC900018

Jolivet, L., Romagny, A., Gorini, C., Maillard, A., Thinon, I., Couëffé, R., et al. (2020). Fast dismantling of a mountain belt by mantle flow: Late-orogenic evolution of Pyrenees and Liguro-Provençal rifting. *Tectonophysics*, *776*, 228312. https://doi.org/10.1016/j.tecto.2019.228312

Jolivet, M., Labaume, P., Monié, P., Brunel, M., Arnaud, N., & Campani, M. (2007). Thermochronology constraints for the propagation sequence of the south Pyrenean basement thrust system (France-Spain). *Tectonics*, *26*(5), TC5007. https://doi.org/10.1029/2006TC002080

Jullien-Sicre, A., Missenard, Y., Blaise, T., Augier, R., Parizot, O., & Haurine, F. (2025). U-Pb on syn-kinematic calcite, Pyrenees, France [Dataset]. *Mendeley Data*. https://doi.org/10.17632/8mr86grhnk.1

Kley, J., & Voigt, T. (2008). Late Cretaceous intraplate thrusting in central Europe: Effect of Africa-Iberia-Europe convergence, not Alpine collision. *Geology*, *36*(11), 839. https://doi.org/10.1130/G24930A.1

Labaume, P., Meresse, F., Jolivet, M., Teixell, A., & Lahfid, A. (2016). Tectonothermal history of an exhumed thrust-sheet-top basin: An example from the south Pyrenean thrust belt. *Tectonics*, *35*(5), 1280–1313. https://doi.org/10.1002/2016TC004192

Labaume, P., Séguret, M., & Seyve, C. (1985). Evolution of a turbiditic foreland basin and analogy with an accretionary prism: Example of the Eocene South-Pyrenean Basin. *Tectonics*, *4*(7), 661–685. https://doi.org/10.1029/TC004i007p00661

Labaume, P., & Teixell, A. (2018). 3D structure of subsurface thrusts in the eastern Jaca Basin, southern Pyrenees. *Geológica Acta*.

Lacombe, O., Beaudoin, N. E., Hoareau, G., Labeur, A., Pecheyran, C., & Callot, J.-P. (2021). Dating folding beyond folding, from layer-parallel shortening to fold tightening, using mesostructures: Lessons from the Apennines, Pyrenees, and Rocky Mountains. *Solid Earth*, *12*(10), 2145–2157. https://doi.org/10.5194/se-12-2145-2021

Lacombe, O., & Jolivet, L. (2005). Structural and kinematic relationships between Corsica and the Pyrenees-Provence domain at the time of the Pyrenean orogeny. *Tectonics*, *24*(1), TC1003. https://doi.org/10.1029/2004TC001673

Lacombe, O., & Obert, D. (2000). Héritage structural et déformation de couverture: Plissement et fracturation tertiaires dans l'Ouest du bassin de Paris. *Comptes Rendus de l'Academie des Sciences - Series IIA: Earth and Planetary Science*, *330*(11), 793–798. https://doi.org/10.1016/S1251-8050(00)00228-7

Lagabrielle, Y., & Bodinier, J. (2008). Submarine reworking of exhumed subcontinental mantle rocks: Field evidence from the Lherz peridotites, French Pyrenees. *Terra Nova*, *20*(1), 11–21. https://doi.org/10.1111/j.1365-3121.2007.00781.x

Lagabrielle, Y., Labaume, P., & De Saint Blanquat, M. (2010). Mantle exhumation, crustal denudation, and gravity tectonics during Cretaceous rifting in the Pyrenean realm (SW Europe): Insights from the geological setting of the lherzolite bodies. *Tectonics*, *29*(4), TC4012. https://doi.org/10.1029/2009TC002588

Larrasoaña, J. C., Parés, J. M., Millán, H., Del Valle, J., & Pueyo, E. L. (2003). Paleomagnetic, structural, and stratigraphic constraints on transverse fault kinematics during basin inversion: The Pamplona Fault (Pyrenees, north Spain). *Tectonics*, *22*(6), 2002TC001446. https://doi.org/10.1029/2002TC001446

Laumonier, B., Marignac, C., & Kister, P. (2010). Polymetamorphism and crustal evolution of the eastern Pyrenees during the Late Carboniferous Variscan orogenesis. *Bulletin de la Societe Geologique de France*, *181*(5), 411–428. https://doi.org/10.2113/gssgfbull.181.5.411

Lawson, M., Shenton, B. J., Stolper, D. A., Eiler, J. M., Rasbury, E. T., Becker, T. P., et al. (2018). Deciphering the diagenetic history of the El Abra Formation of eastern Mexico using reordered clumped isotope temperatures and U-Pb dating. *GSA Bulletin*, *130*(3–4), 617–629. https://doi.org/10.1130/B31656.1

Lopez-Blanco, M., Marzo, M., Burbank, D. W., VergeÂs, J., Roca, E., AnadoÂn, P., & PinÄa, J. (2000). Tectonic and climatic controls on the development of foreland fan deltas: Montserrat and Sant LlorencË del Munt systems (Middle Eocene, Ebro Basin, NE Spain). *Sedimentary Geology*, *138*(1–4), 17–39. https://doi.org/10.1016/s0037-0738(00)00142-1

Macchiavelli, C., Vergés, J., Schettino, A., Fernàndez, M., Turco, E., Casciello, E., et al. (2017). A New southern North Atlantic isochron map: Insights into the drift of the Iberian plate since the Late Cretaceous. *Journal of Geophysical Research: Solid Earth*, *122*(12), 9603–9626. https://doi.org/10.1002/2017JB014769

McClay, K., Muñoz, J.-A., & García-Senz, J. (2004). Extensional salt tectonics in a contractional orogen: A newly identified tectonic event in the Spanish Pyrenees. *Geology*, *32*(9), 737. https://doi.org/10.1130/G20565.1

Milesi, G., Monié, P., Soliva, R., Münch, P., Valla, P. G., Brichau, S., et al. (2022). Deciphering the Cenozoic exhumation history of the Eastern Pyrenees along a crustal-scale normal fault using low-temperature thermochronology. *Tectonics*, *41*(4), e2021TC007172. https://doi.org/10.1029/2021TC007172

Monchal, V., Drost, K., & Chew, D. (2023). Precise U-Pb dating of incremental calcite slickenfiber growth: Evidence for far-field Eocene fold reactivation in Ireland. *Geology*, *51*(7), 611–615. https://doi.org/10.1130/G50906.1

Mouthereau, F., Angrand, P., Jourdon, A., Ternois, S., Fillon, C., Calassou, S., et al. (2021). Cenozoic mountain building and topographic evolution in Western Europe: Impact of billions of years of lithosphere evolution and plate kinematics. *BSGF - Earth Sciences Bulletin*, *192*(1), 56. https://doi.org/10.1051/bsgf/2021040

Mouthereau, F., Filleaudeau, P.-Y., Vacherat, A., Pik, R., Lacombe, O., Fellin, M. G., et al. (2014). Placing limits to shortening evolution in the Pyrenees: Role of margin architecture and implications for the Iberia/Europe convergence: Plate convergence in the Pyrenees. *Tectonics*, *33*(12), 2283–2314. https://doi.org/10.1002/2014TC003663

Muñoz, J. A. (1992). Evolution of a continental collision belt: ECORS-Pyrenees crustal balanced cross-section. In K. R. McClay (Ed.), *Thrust tectonics* (pp. 235–246). Springer Netherlands. https://doi.org/10.1007/978-94-011-3066-0_21



19449194, 2025, 2, Downloaded from https://agupubs.onlinelibrary.wiley.com/doi/10.1029/2024TC008634 by Portail BibCNRS INSU, Wiley Online Library on [03/03/2025]. See the Terms and Conditions (https://onlinelibrary.wiley.com/terms-and-conditions) on Wiley Online Library for rules of use; OA articles are governed by the applicable Creative Commons License

Muñoz-López, D., Cruset, D., Vergés, J., Cantarero, I., Benedicto, A., Mangenot, X., et al. (2022). Spatio-temporal variation of fluid flow behavior along a fold: The Bóixols-Sant Corneli anticline (Southern Pyrenees) from U–Pb dating and structural, petrographic and geochemical constraints. *Marine and Petroleum Geology*, *143*, 105788. https://doi.org/10.1016/j.marpetgeo.2022.105788

Navabpour, P., Malz, A., Kley, J., Siegburg, M., Kasch, N., & Ustaszewski, K. (2017). Intraplate brittle deformation and states of paleostress constrained by fault kinematics in the central German platform. *Tectonophysics*, *694*, 146–163. https://doi.org/10.1016/j.tecto.2016.11.033

Nielsen, S. B., Thomsen, E., Hansen, D. L., & Clausen, O. R. (2005). Plate-wide stress relaxation explains European Palaeocene basin inversions. *Nature*, *435*(7039), 195–198. https://doi.org/10.1038/nature03599

Oliva-Urcia, B., Beamud, E., Arenas, C., Pueyo, E. L., Garcés, M., Soto, R., et al. (2019). Dating the northern deposits of the Ebro foreland basin; implications for the kinematics of the SW Pyrenean front. *Tectonophysics*, *765*, 11–34. https://doi.org/10.1016/j.tecto.2019.05.007

Ortiz, A., Guillocheau, F., Lasseur, E., Briais, J., Robin, C., Serrano, O., & Fillon, C. (2020). Sediment routing system and sink preservation during the post-orogenic evolution of a retro-foreland basin: The case example of the North Pyrenean (Aquitaine, Bay of Biscay) Basins. *Marine and Petroleum Geology*, *112*, 104085. https://doi.org/10.1016/j.marpetgeo.2019.104085

Pagel, M., Bonifacie, M., Schneider, D. A., Gautheron, C., Brigaud, B., Calmels, D., et al. (2018). Improving paleohydrological and diagenetic reconstructions in calcite veins and breccia of a sedimentary basin by combining $\Delta_{47}$ temperature, $\delta^{18}O_{water}$ and U-Pb age. *Chemical Geology*, *481*, 1–17. https://doi.org/10.1016/j.chemgeo.2017.12.026

Parizot, O., Missenard, Y., Barbarand, J., Blaise, T., Benedicto, A., Haurine, F., & Sarda, P. (2022). How sensitive are intraplate inherited structures? Insight from the Cévennes Fault System (Languedoc, SE France). *Geological Magazine*, *159*(11–12), 1–13. https://doi.org/10.1017/S0016756822000152

Parizot, O., Missenard, Y., Haurine, F., Blaise, T., Barbarand, J., Benedicto, A., & Sarda, P. (2021). When did the Pyrenean shortening end? Insight from U-Pb geochronology of syn-faulting calcite (Corbières area, France). *Terra Nova*, *33*(6), 551–559. https://doi.org/10.1111/ter.12547

Parizot, O., Missenard, Y., Vergely, P., Haurine, F., Noret, A., Delpech, G., et al. (2020). Tectonic Record of Deformation in Intraplate Domains: Case Study of Far-Field Deformation in the Grands Causses Area, France. *Geofluids*, *2020*, 1–19. https://doi.org/10.1155/2020/7598137

Parrish, R. R., Parrish, C. M., & Lasalle, S. (2018). Vein calcite dating reveals Pyrenean orogen as cause of Paleogene deformation in southern England. *Journal of the Geological Society*, *175*(3), 425–442. https://doi.org/10.1144/jgs2017-107

Paton, C., Hellstrom, J., Paul, B., Woodhead, J., & Hergt, J. (2011). Iolite: Freeware for the visualisation and processing of mass spectrometric data. *Journal of Analytical Atomic Spectrometry*, *26*(12), 2508. https://doi.org/10.1039/c1ja10172b

Platt, J., Behrmann, J., Cunningham, P., Dewey, J., Helman, M., Parish, M., et al. (1989). Kinematics of the Alpine arc and the motion history of Adria. *Nature*, *337*(6203), 158–161. https://doi.org/10.1038/337158a0

Puigdefàbregas, C., & Souquet, P. (1986). Tecto-sedimentary cycles and depositional sequences of the Mesozoic and Tertiary from the Pyrenees. *Tectonophysics*, *129*(1–4), 173–203. https://doi.org/10.1016/0040-1951(86)90251-9

Ring, U., & Gerdes, A. (2016). Kinematics of the Alpenrhein-Bodensee graben system in the Central Alps: Oligocene/Miocene transtension due to formation of the Western Alps arc. *Tectonics*, *35*(6), 1367–1391. https://doi.org/10.1002/2015TC004085

Roberts, N. M. W., Rasbury, E. T., Parrish, R. R., Smith, C. J., Horstwood, M. S. A., & Condon, D. J. (2017). A calcite reference material for LA-ICP-MS U-Pb geochronology. *Geochemistry, Geophysics, Geosystems*, *18*(7), 2807–2814. https://doi.org/10.1002/2016GC006784

Roberts, N. M. W., Žák, J., Vacek, F., & Sláma, J. (2021). No more blind dates with calcite: Fluid-flow vs. fault-slip along the Očkov thrust, Prague Basin. *Geoscience Frontiers*, *12*(4), 101143. https://doi.org/10.1016/j.gsf.2021.101143

Rosenbaum, G., Lister, G. S., & Duboz, C. (2002). Relative motions of Africa, Iberia and Europe during Alpine orogeny. *Tectonophysics*, *359*(1–2), 117–129. https://doi.org/10.1016/S0040-1951(02)00442-0

Rougier, G., Ford, M., Christophoul, F., & Bader, A.-G. (2016). Stratigraphic and tectonic studies in the central Aquitaine Basin, northern Pyrenees: Constraints on the subsidence and deformation history of a retro-foreland basin. *Comptes Rendus Geoscience*, *348*(3–4), 224–235. https://doi.org/10.1016/j.crte.2015.12.005

Rushlow, C. R., Barnes, J. B., Ehlers, T. A., & Vergés, J. (2013). Exhumation of the southern Pyrenean fold-thrust belt (Spain) from orogenic growth to decay. *Tectonics*, *32*(4), 843–860. https://doi.org/10.1002/tect.20030

Sainz, A. M. C., & Faccenna, C. (2001). Tertiary compressional deformation of the Iberian plate. *Terra Nova*, *13*(4), 281–288. https://doi.org/10.1046/j.1365-3121.2001.00355.x

Sartégou, A., Bourlès, D. L., Blard, P.-H., Braucher, R., Tibari, B., Zimmermann, L., et al. (2018). Deciphering landscape evolution with karstic networks: A Pyrenean case study. *Quaternary Geochronology*, *43*, 12–29. https://doi.org/10.1016/j.quageo.2017.09.005

Saura, E., Ardèvol i Oró, L., Teixell, A., & Vergés, J. (2016). Rising and falling diapirs, shifting depocenters, and flap overturning in the Cretaceous Sopeira and Sant Gervàs subbasins (Ribagorça Basin, southern Pyrenees). *Tectonics*, *35*(3), 638–662. https://doi.org/10.1002/2015TC004001

Scheck-Wenderoth, M., & Lamarche, J. (2005). Crustal memory and basin evolution in the Central European Basin System—New insights from a 3D structural model. *Tectonophysics*, *397*(1–2), 143–165. https://doi.org/10.1016/j.tecto.2004.10.007

Schettino, A., & Turco, E. (2011). Tectonic history of the western Tethys since the Late Triassic. *Geological Society of America Bulletin*, *123*(1–2), 89–105. https://doi.org/10.1130/B30064.1

Séranne, M. (1999). The Gulf of Lion continental margin (NW Mediterranean) revisited by IBS: An overview. *Geological Society, London, Special Publications*, *156*(1), 15–36. https://doi.org/10.1144/GSL.SP.1999.156.01.03

Séranne, M., Couëffé, R., Husson, E., Baral, C., & Villard, J. (2021). The transition from Pyrenean shortening to Gulf of Lion rifting in Languedoc (South France) – A tectonic-sedimentation analysis. *BSGF - Earth Sciences Bulletin*, *192*, 27. https://doi.org/10.1051/bsgf/2021017

Serrano, O., Delmas, J., Hanot, F., Vially, R., Herbin, J. P., Houel, P., & Tourlière, B. (2006). *Le Bassin d'Aquitaine: valorisation des données sismiques, cartographie structurale et potentiel pétrolier*. BRGM. https://doi.org/10.13140/2.1.1304.2241

Sinclair, H. D. (2005). Asymmetric growth of the Pyrenees revealed through measurement and modeling of orogenic fluxes. *American Journal of Science*, *305*(5), 369–406. https://doi.org/10.2475/ajs.305.5.369

Sokoutis, D., Burg, J.-P., Bonini, M., Corti, G., & Cloetingh, S. (2005). Lithospheric-scale structures from the perspective of analogue continental collision. *Tectonophysics*, *406*(1–2), 1–15. https://doi.org/10.1016/j.tecto.2005.05.025

Souquet, P., Debroas, E. J., Boirie, J.-M., Pons, P., Fixari, G., Roux, J.-C., et al. (1985). Le groupe du Flysch Noir (Albo-Cenomanien) dans les Pyrenees. *Bulletin des Centres de Recherches Exploration-Production Elf-Aquitaine*, *9*, 183–252.

Sutherland, R., Collot, J., Bache, F., Henrys, S., Barker, D., Browne, G. H., et al. (2017). Widespread compression associated with Eocene Tonga-Kermadec subduction initiation. *Geology*, *45*(4), 355–358. https://doi.org/10.1130/G38617.1

Sztrákos, K., Blondeau, A., & Hottinger, L. (2010). Lithostratigraphie et biostratigraphie des formations marines paléocènes et éocènes nord-aquitaines (bassins de Contis et Parentis, seuil et plate-forme nord-aquitains), Foraminifères éocènes du bassin d'Aquitaine. *Géologie de la France*, *2*, 3–52.



19449194, 2025, 2, Downloaded from https://agupubs.onlinelibrary.wiley.com/doi/10.1029/2024TC008634 by Portail BibCNRS INSU, Wiley Online Library on [03/03/2025]. See the Terms and Conditions (https://onlinelibrary.wiley.com/terms-and-conditions) on Wiley Online Library for rules of use; OA articles are governed by the applicable Creative Commons License

Taillefer, A., Milesi, G., Soliva, R., Monnier, L., Delorme, P., Guillou-Frottier, L., & Le Goff, E. (2021). Polyphased brittle deformation around a crustal fault: A multi-scale approach based on remote sensing and field data on the mountains surrounding the Têt hydrothermal system (Eastern Pyrénées, France). *Tectonophysics*, *804*, 228710. https://doi.org/10.1016/j.tecto.2020.228710

Tambareau, Y., Crochet, B., Villatte, J., & Deramond, J. (1995). Evolution tectono-sedimentaire du versant nord des Pyrenees centre-orientales au Paleocene et a l'Eocene inferieur. *Bulletin de la Societe Geologique de France*, *166*(4), 375–387. https://doi.org/10.2113/gssgfbull.166.4.375

Teixell, A. (1996). The Ansó transect of the southern Pyrenees: Basement and cover thrust geometries. *Journal of the Geological Society*, *153*(2), 301–310. https://doi.org/10.1144/gsjgs.153.2.0301

Teixell, A., Bertotti, G., De Lamotte, D. F., & Charroud, M. (2009). The geology of vertical movements of the lithosphere: An overview. *Tectonophysics*, *475*(1), 1–8. https://doi.org/10.1016/j.tecto.2009.08.018

Teixell, A., Labaume, P., Ayarza, P., Espurt, N., De Saint Blanquat, M., & Lagabrielle, Y. (2018). Crustal structure and evolution of the Pyrenean-Cantabrian belt: A review and new interpretations from recent concepts and data. *Tectonophysics*, *724–725*, 146–170. https://doi.org/10.1016/j.tecto.2018.01.009

Uzel, J., Nivière, B., & Lagabrielle, Y. (2019). Fluvial incisions in the Noth-Western Pyrenees (Aspe Valley): Dissection of a former planation surface and some tectonic implications. *Terra Nova*, *32*(1), 11–22. https://doi.org/10.1111/ter.12431

Vandenberghe, N., Van Simaeys, S., Steurbaut, E., Jagt, J. W. M., & Felder, P. J. (2004). Stratigraphic architecture of the Upper Cretaceous and Cenozoic along the southern border of the North Sea Basin in Belgium. *Netherlands Journal of Geosciences - Geologie En Mijnbouw*, *83*(3), 155–171. https://doi.org/10.1017/S0016774600020229

Vergely, P., & Xu, W. L. (1988). Les escaliers d'accrétion de calcite: Un exemple de déformation par fracturation-cristallisation accompagnant le glissement sur les failles. *Geodinamica Acta*, *2*(4), 207–217. https://doi.org/10.1080/09853111.1988.11105168

Vergés, J., Feràndez, M., & Martinez Rius, A. (2002). The Pyrenean orogen: Pre-, syn-, and post-collisional evolution. *Journal of the Virtual Explorer*, *8*, 55–74. https://doi.org/10.3809/jvirtex.2002.00058

Vergés, J., Millán, H., Roca, E., Muñoz, J. A., Marzo, M., Cirés, J., et al. (1995). Eastern Pyrenees and related foreland basins: Pre-syn- and post-collisional crustal-scale cross-sections. *Marine and Petroleum Geology*, *12*(8), 903–915. https://doi.org/10.1016/0264-8172(95)98854-X

Vermeesch, P. (2018). IsoplotR: A free and open toolbox for geochronology. *Geoscience Frontiers*, *9*(5), 1479–1493. https://doi.org/10.1016/j.gsf.2018.04.001

Vissers, R. L. M. (1992). Variscan extension in the Pyrenees. *Tectonics*, *11*(6), 1369–1384. https://doi.org/10.1029/92TC00823

Willett, S., Beaumont, C., & Fullsack, P. (1993). Mechanical model for the tectonics of doubly vergent compressional orogens. *Geology*, *21*(4), 371. https://doi.org/10.1130/0091-7613(1993)021<0371:MMFTTO>2.3.CO;2

Willingshofer, E., & Sokoutis, D. (2009). Decoupling along plate boundaries: Key variable controlling the mode of deformation and the geometry of collisional mountain belts. *Geology*, *37*(1), 39–42. https://doi.org/10.1130/G25321A.1

Willingshofer, E., Sokoutis, D., Luth, S. W., Beekman, F., & Cloetingh, S. (2013). Subduction and deformation of the continental lithosphere in response to plate and crust-mantle coupling. *Geology*, *41*(12), 1239–1242. https://doi.org/10.1130/G34815.1

Woodhead, J., Horstwood, M. S. A., & Cottle, J. (2016). Advances in isotope ratio determination by laser ablation inductively coupled plasma mass spectrometry (LA–ICP–MS). *Geoscience Frontiers*, *9*, 1479–1493.

Ziegler, P. A. (1998). Collisional intraplate deformation. *GFF*, *120*(2), 249–256. https://doi.org/10.1080/11035899801202249

Ziegler, P. A., Cloetingh, S., & Van Wees, J.-D. (1995). Dynamics of intra-plate compressional deformation: The Alpine foreland and other examples. *Tectonophysics*, *252*(1–4), 7–59. https://doi.org/10.1016/0040-1951(95)00102-6

## References From the Supporting Information

Jochum, K. P., Weis, U., Stoll, B., Kuzmin, D., Yang, Q., Raczek, I., et al. (2011). Determination of Reference Values for NIST SRM 610-617 Glasses Following ISO Guidelines. *Geostandards and Geoanalytical Research*, *35*(4), 397–429. https://doi.org/10.1111/j.1751-908X.2011.00120.x

Nuriel, P., Wotzlaw, J.-F., Ovtcharova, M., Vaks, A., Stremtan, C., Šala, M., et al. (2020). *The use of ASH-15 flowstone as a matrix-matched reference material for laser-ablation U-Pb geochronology of calcite (preprint)*. SIMS, LA-ICP-MS. https://doi.org/10.5194/gchron-2020-22



19449194, 2025, 2, Downloaded from https://agupubs.onlinelibrary.wiley.com/doi/10.1029/2024TC008634 by Portail BibCNRS INSU, Wiley Online Library on [03/03/2025]. See the Terms and Conditions (https://onlinelibrary.wiley.com/terms-and-conditions) on Wiley Online Library for rules of use; OA articles are governed by the applicable Creative Commons License